



SUCNR1 controls an anti-inflammatory program in macrophages to regulate the metabolic response to obesity

Noelia Keiran^{1,2,11}, Victoria Ceperuelo-Mallafre^{1,2,11}, Enrique Calvo^{1,2}, Maria Isabel Hernández-Alvarez^{1,2,3}, Miriam Ejarque^{1,2}, Catalina Núñez-Roa^{1,2}, Daniel Horrillo⁴, Elsa Maymó-Masip^{1,2}, M. Mar Rodríguez^{1,2}, Rosa Fradera⁵, Juan Vladimir de la Rosa^{6,7}, Rosa Jorba⁸, Ana Megia^{1,2}, Antonio Zorzano^{2,3,9}, Gema Medina-Gómez⁴, Carolina Serena^{1,2}, Antonio Castrillo^{6,7}, Joan Vendrell ^{1,2,10,12*} and Sonia Fernández-Veledo ^{1,2,12*}

Succinate is a signaling metabolite sensed extracellularly by succinate receptor 1 (SUCNR1). The accumulation of succinate in macrophages is known to activate a pro-inflammatory program; however, the contribution of SUCNR1 to macrophage phenotype and function has remained unclear. Here we found that activation of SUCNR1 had a critical role in the anti-inflammatory responses in macrophages. Myeloid-specific deficiency in SUCNR1 promoted a local pro-inflammatory phenotype, disrupted glucose homeostasis in mice fed a normal chow diet, exacerbated the metabolic consequences of diet-induced obesity and impaired adipose-tissue browning in response to cold exposure. Activation of SUCNR1 promoted an anti-inflammatory phenotype in macrophages and boosted the response of these cells to type 2 cytokines, including interleukin-4. Succinate decreased the expression of inflammatory markers in adipose tissue from lean human subjects but not that from obese subjects, who had lower expression of SUCNR1 in adipose-tissue-resident macrophages. Our findings highlight the importance of succinate-SUCNR1 signaling in determining macrophage polarization and assign a role to succinate in limiting inflammation.

Traditionally considered an energetic metabolite of the mitochondrial tricarboxylic acid cycle, succinate has recently emerged as a metabolic signal governing local stress, tissue damage and immunologic danger^{1–4}. Thus, in certain activated innate immune cells or in cells relying on anaerobic glycolysis in hypoxia, the amount of mitochondrial succinate increases⁵ and is then released into the cytosol, where its accumulation is directly related to protein succinylation, stabilization of the transcription factor HIF-1 α , epigenetic regulation and reactive oxygen species production^{1,3,5}.

Succinate can also be released to the extracellular space through plasma-membrane transporters of the SLC13 family, by poorly understood processes^{4,6}. Elevated amounts of circulating succinate occur in some physiological conditions, such as endurance exercise⁷ and in certain pathologies, including hypertension⁸, ischemic heart disease⁹, type 2 diabetes mellitus^{8,10} and obesity^{8,11}. Extracellular succinate binds its receptor succinate receptor 1 (SUCNR1, also known as GPR91)¹² on the plasma membrane of a broad range of cells^{13,14}. To date, activation of SUCNR1 by extracellular succinate has been associated with pathological cardiomyocyte hypertrophy⁹, normal retinal development and proliferative ischemic retinopathy¹⁵, pathogenesis of diabetic nephropathy by activating renin-angiotensin

system^{4,6,16}, hepatic fibrosis through activation of α -SMA production in stellate cells¹⁷ and adipose tissue expansion by SUCNR1-dependent antilipolytic effects in adipocytes¹⁸, among others.

The succinate-SUCNR1 signaling axis has a complex role in immune responses^{19,20}. Dendritic cells sense immunological danger through SUCNR1, to enhance antigen-presenting functions required for optimal immune activation^{2,21}. Further, the absence of SUCNR1 produces a hyperactive mast cell phenotype²². While succinate is known to be released by lipopolysaccharide (LPS)-activated pro-inflammatory macrophages²³, the role of SUCNR1 in macrophage plasticity remains largely unknown. Thus, despite early reports that SUCNR1 activation boosts pro-inflammatory responses in macrophages during antigen-induced arthritis²³, SUCNR1-deficient peritoneal macrophages have a similar cytokine profile as those derived from wild-type animals, both in basal and in LPS-stimulated conditions¹⁰. Moreover, recent reports showed that extracellular succinate might also mediate anti-inflammatory responses in neural stem cells²⁴. Indeed, SUCNR1 has been described as a major driver of microbiota-triggered type 2 immunity in the intestine²⁵.

There is strong evidence that succinate-SUCNR1 signaling serves as a link between metabolic stress and inflammation;

¹Unitat de Recerca, Hospital Universitari de Tarragona Joan XXIII, Institut d' Investigació Sanitària Pere Virgili, Tarragona, Spain. ²CIBER de Diabetes y Enfermedades Metabólicas Asociadas (CIBERDEM), Instituto de Salud Carlos III, Madrid, Spain. ³Institute for Research in Biomedicine (IRB Barcelona), The Barcelona Institute of Science and Technology, Barcelona, Spain. ⁴Departamento de Ciencias Básicas de la Salud, Área de Bioquímica y Biología Molecular, Universidad Rey Juan Carlos, Madrid, Spain. ⁵General and Digestive Surgery Service, Hospital St. Pau i Sta Tecla, Institut d' Investigació Sanitària Pere Virgili, Tarragona, Spain. ⁶Instituto de Investigaciones Biomédicas "Alberto Sols" CSIC-UAM, Madrid, Spain. ⁷Unidad de Biomedicina (Unidad Asociada al CSIC), Instituto Universitario de Investigaciones Biomédicas y Sanitaria (IUBIS), Universidad de Las Palmas de Gran Canaria, Las Palmas, Spain. ⁸General and Digestive Surgery Service, Hospital Universitari de Tarragona Joan XXIII, Institut d' Investigació Sanitària Pere Virgili, Tarragona, Spain. ⁹Departament de Bioquímica i Biomedicina Molecular, Facultat de Biologia, Barcelona, Spain. ¹⁰Universitat Rovira i Virgili, Tarragona, Spain. ¹¹These authors contributed equally: Noelia Keiran, Victoria Ceperuelo-Mallafre. ¹²These authors jointly supervised this work: Joan Vendrell, Sonia Fernández-Veledo.

*e-mail: jvo@comt.es; sonia.fernandezveledo@gmail.com

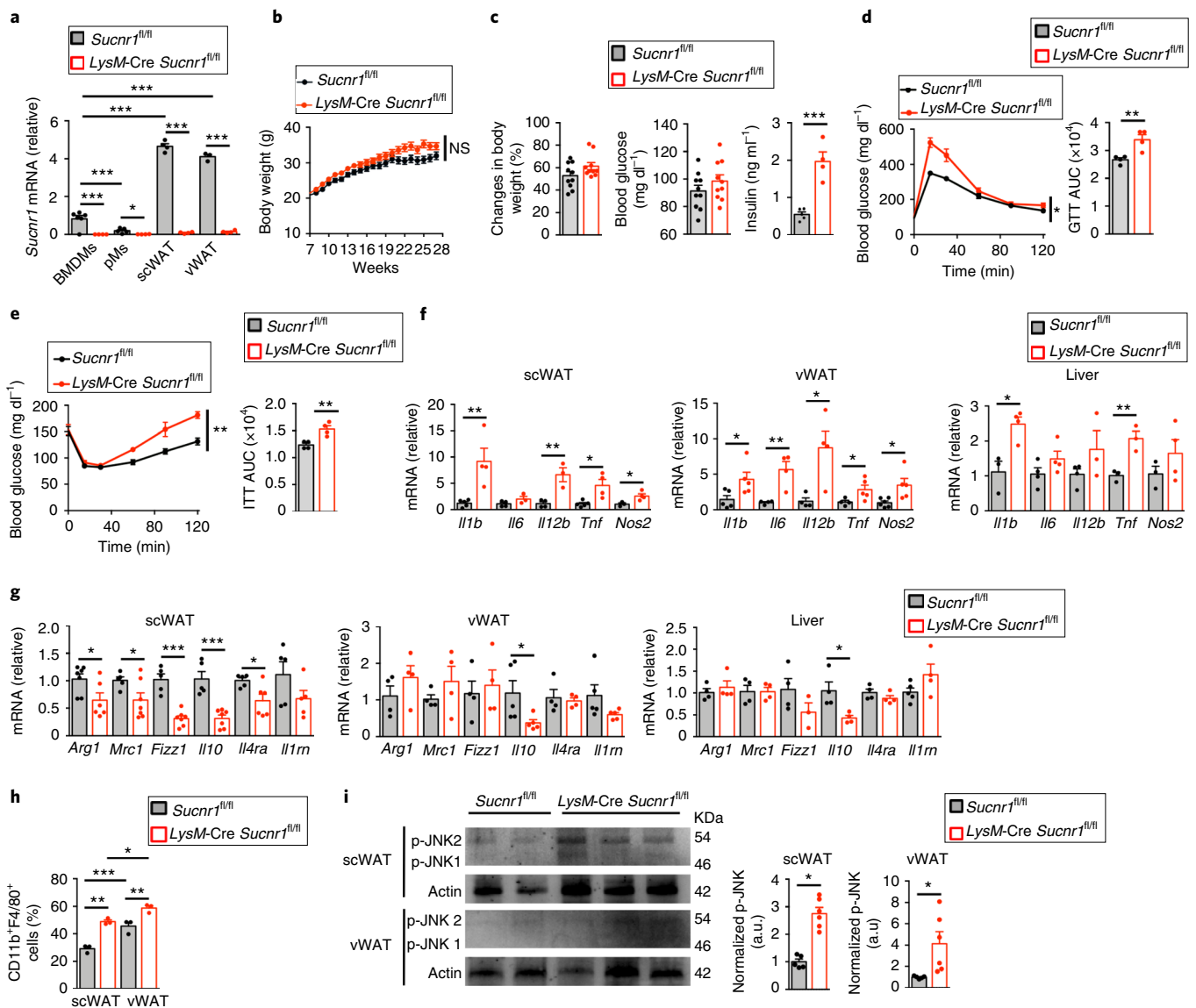


Fig. 1 | *LysM-Cre Sucnr1*^{fl/fl} mice fed a NCD show tissue inflammation and glucose intolerance. **a**, qPCR analysis of *Sucnr1* mRNA in BMDMs, peritoneal macrophages (pMs), scWAT ATMs and vWAT ATMs in *LysM-Cre Sucnr1*^{fl/fl} mice and age-matched *Sucnr1*^{fl/fl} littermates (BMDMs and peritoneal macrophages $n = 5$ or 4 ; scWAT $n = 4$; vWAT $n = 3$ or 4 , for *Sucnr1*^{fl/fl} and *LysM-Cre Sucnr1*^{fl/fl} respectively; biologically independent samples). Results are transformed as $\log_2(\text{value} + 1)$ relative to BMDMs from *Sucnr1*^{fl/fl} mice, set as 1. **b**, Body weight progression. **c**, Changes in body weight and fasting serum glucose as in **a** from two independent experiments ($n = 10$ mice). Serum insulin levels as in **a** ($n = 5$ for *Sucnr1*^{fl/fl} and $n = 4$ for *LysM-Cre Sucnr1*^{fl/fl} mice). **d, e**, GTT (**d**), ITT (**e**) and their respective area under the curve (AUC) as in **a** ($n = 4$ mice). **f, g**, qPCR analysis of pro-inflammatory (**f**; $n = 6$ for *Sucnr1*^{fl/fl} and $n = 5$ for *LysM-Cre Sucnr1*^{fl/fl} mice) and anti-inflammatory genes (**g**; $n = 7$ mice) as in **a** from two independent experiments. **h**, Abundance of CD11b⁺F4/80⁺ cells assessed by flow cytometry in scWAT and vWAT SVF ($n = 3$ biologically independent samples). **i**, Immunoblot analysis of phosphorylated (p-)JNK1/2 protein. β -actin was used as a loading control. Representative image and densitometry analysis (a.u., arbitrary units) ($n = 5$ per *Sucnr1*^{fl/fl} and $n = 6$ per *LysM-Cre Sucnr1*^{fl/fl} biologically independent samples). Uncropped blots are provided in source data. All data are shown as mean \pm s.e.m.; * $P < 0.05$; ** $P < 0.01$; *** $P < 0.001$; NS, non-significant (two-tailed unpaired *t*-test in bar graphs and two-way analysis of variance in body-weight, GTT and ITT curves).

however, whether succinate can be regarded as a harmful signal or has a protective role remains controversial. Because obesity is associated with chronic inflammation, and because macrophages are central mediators in obesity-associated inflammation, here we used mice with conditional inactivation of *Sucnr1* in myeloid cells to investigate the role of succinate–SUCNRI signaling in obesity. We found that SUCNRI modulated the phenotype of bone-marrow-derived macrophages (BMDMs) in a cell-autonomous manner. SUCNRI signaling induced an anti-inflammatory phenotype in adipose-tissue-resident macrophages (ATMs) and dampened tissue inflammation both at steady state and after challenges that

disrupted metabolic homeostasis. Our data strengthen the idea that macrophages have a key role in the pathogenesis of obesity and identify succinate–SUCNRI signaling as a metabolic guardian in inflammatory-associated disorders.

Results

Myeloid *Sucnr1* deficiency provokes inflammation and glucose intolerance. To elucidate the role of succinate–SUCNRI signaling in macrophages, we crossed mice bearing a conditional loxP-flanked ('floxed') allele of *Sucnr1* (*Sucnr1*^{fl/fl}, used as control mice) to transgenic mice expressing bacterial Cre recombinase under the

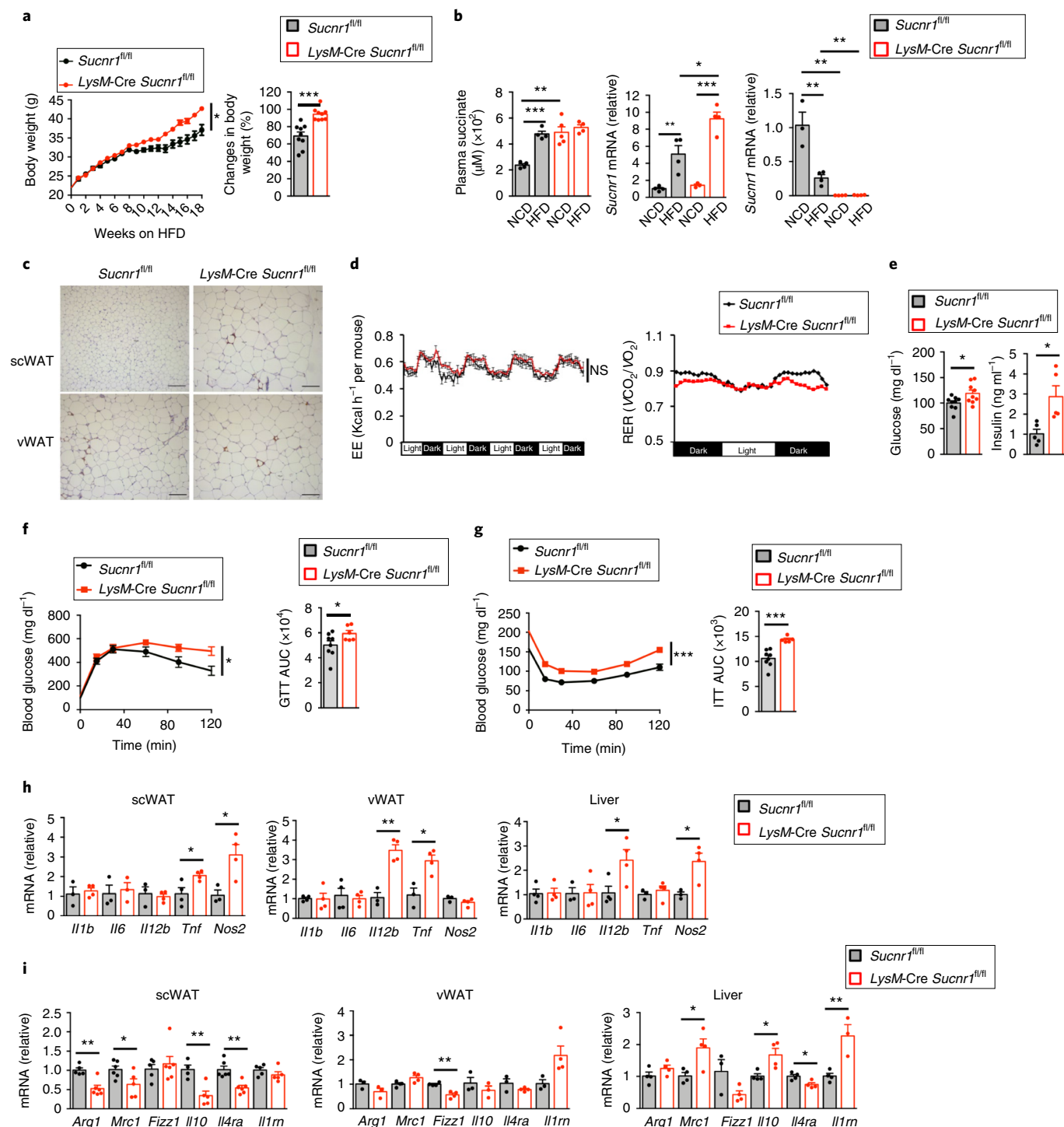


Fig. 2 | *LysM-Cre Sucnr1^{fl/fl}* mice on HFD are prone to develop obesity, glucose intolerance and insulin sensitivity. **a**, Body-weight progression in *LysM-Cre Sucnr1^{fl/fl}* mice and age-matched *Sucnr1^{fl/fl}* littermates fed a HFD for 18 weeks ($n=9$ mice). **b**, Left, fasting plasma succinate in *LysM-Cre Sucnr1^{fl/fl}* and *Sucnr1^{fl/fl}* mice fed a HFD or NCD ($n=4$ for *Sucnr1^{fl/fl}* and $n=5$ for *LysM-Cre Sucnr1^{fl/fl}* on NCD; $n=4$ mice on HFD). Right, qPCR analysis of *Sucnr1* mRNA in scWAT ($n=4$ for *Sucnr1^{fl/fl}* and $n=3$ for *LysM-Cre Sucnr1^{fl/fl}* on NCD; $n=4$ mice on HFD) and scWAT ATMs as in **a** (right) ($n=4$ biologically independent samples). **c**, Immunohistochemical staining of F4/80⁺ cells in scWAT and vWAT as in **a**. Representative images from two independent experiments ($n=4$ mice). Scale bars, 1 mm. **d**, Energy expenditure (EE) (left) and respiratory exchange ratio (RER) (right) during light and dark hours, as in **a** ($n=5$ mice). **e**, Fasting serum glucose ($n=9$ mice) and insulin levels ($n=5$ mice) as in **a**. **f, g**, GTT (**f**; $n=8$ *Sucnr1^{fl/fl}*; $n=6$ *LysM-Cre Sucnr1^{fl/fl}*) and ITT (**g**; $n=8$ *Sucnr1^{fl/fl}*; $n=5$ *LysM-Cre Sucnr1^{fl/fl}*) and their respective area under the curve as in **a**. **h, i**, qPCR analysis of pro-inflammatory (**h**; $n=4$ mice) and anti-inflammatory (**i**; $n=6$ mice) genes in scWAT, vWAT and liver as in **a** from two independent experiments. Results are expressed as mean \pm s.e.m.; * $P < 0.05$; ** $P < 0.01$; *** $P < 0.001$; NS, non-significant (two-tailed unpaired *t*-test in bar graphs and two-way analysis of variance in body-weight, GTT and ITT curves).

control of the lysozyme 2 promoter (*LysM-Cre*) to generate mice with myeloid-cell-specific *Sucnr1* deficiency (hereafter referred to as *LysM-Cre Sucnr1^{fl/fl}*) (Supplementary Fig. 1). *LysM-Cre Sucnr1^{fl/fl}*

mice were born in a Mendelian ratio, and no obvious morphological differences were observed between genotypes (data not shown). Gene analysis showed that expression of *Sucnr1* mRNA was

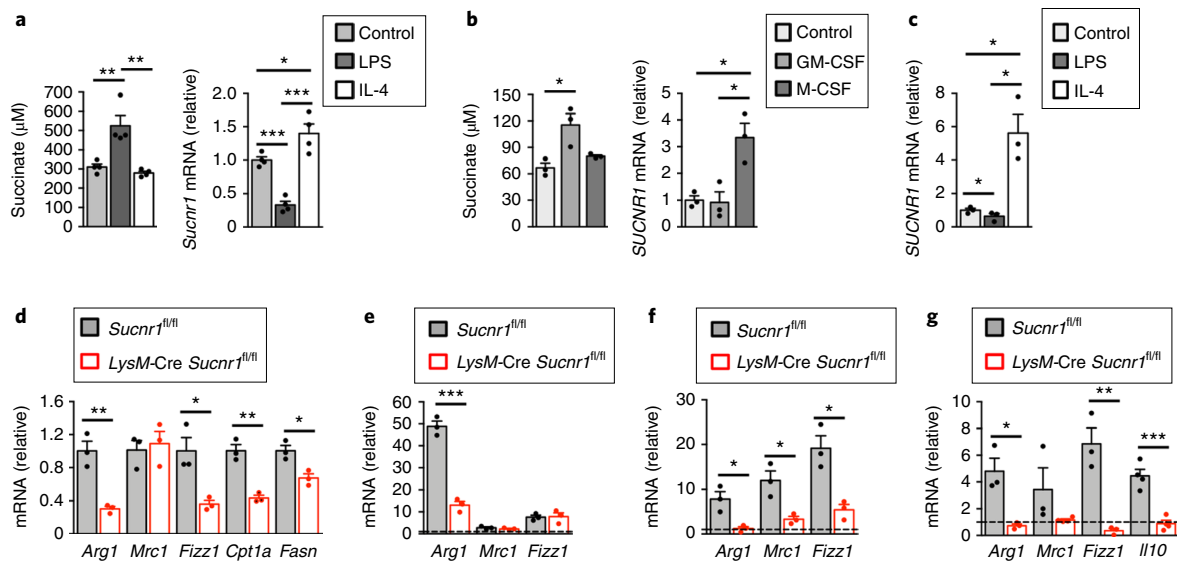


Fig. 3 | Signaling by succinate via SUCNR1 promotes an anti-inflammatory macrophage program in a cell-autonomous manner. **a**, Succinate secretion in 24 h-conditioned medium (left) and *Sucnr1* mRNA expression (right) of peritoneal macrophages from *Sucnr1*^{fl/fl} mice, without stimulation or stimulated with LPS or IL-4 for 6 h ($n = 4$). **b**, Succinate secretion in 24 h-conditioned medium CM (left) and *SUCNR1* mRNA expression (right) in hPBMCs non-differentiated (control) or differentiated with GM-CSF or M-CSF for 7 d ($n = 3$). **c**, *SUCNR1* mRNA expression of hPBMCs differentiated with M-CSF, and then unstimulated or stimulated for 24 h with LPS or IL-4 ($n = 3$). **d**, qPCR mRNA analysis of selected genes in peritoneal macrophages from *Sucnr1*^{fl/fl} and *LysM-Cre Sucnr1*^{fl/fl} mice ($n = 3$). **e**, qPCR analysis in peritoneal macrophages after IL-4 stimulation for 6 h ($n = 3$). Results are expressed relative to a basal state represented as 1. **f**, qPCR mRNA analysis in *Sucnr1*^{fl/fl} and *LysM-Cre Sucnr1*^{fl/fl} BMDMs stimulated with M-CSF for 7 d ($n = 3$), relative to their respective basal expression as 1. **g**, qPCR mRNA analysis in BMDM^{M-CSF} stimulated with succinate (200 µM) overnight ($n = 4$). **a–f**, n represents biologically independent samples. Data are shown as mean \pm s.e.m.; * $P < 0.05$; ** $P < 0.01$; *** $P < 0.001$ (two-tailed unpaired t -test).

negligible in BMDMs, elicited-peritoneal macrophages and adipose-tissue-resident macrophages (ATMs) from *LysM-Cre Sucnr1*^{fl/fl} mice (Fig. 1a). No significant differences were found between *LysM-Cre Sucnr1*^{fl/fl} and *Sucnr1*^{fl/fl} mice in body and fat-pad weight (Fig. 1b,c and Supplementary Fig. 2a) and energy metabolic parameters measured by indirect calorimetry (Supplementary Fig. 2b,c) when they were fed a normal chow diet (NCD) for 20 weeks. Serum glucose was also comparable between genotypes (Fig. 1c); however, insulin levels were higher in *LysM-Cre Sucnr1*^{fl/fl} mice (Fig. 1c), and they also exhibited impaired glucose tolerance (Fig. 1d) and insulin sensitivity (Fig. 1e) compared with *Sucnr1*^{fl/fl} mice. Next, we evaluated the inflammatory status of white adipose tissue (WAT) and liver in *LysM-Cre Sucnr1*^{fl/fl} and *Sucnr1*^{fl/fl} mice. Gene analysis showed that the expression of genes typically linked to the development of insulin resistance, *Il1b*, *Il6*, *Il12b*, *Tnf* and *Nos2*, was higher in the subcutaneous (sc) and visceral (v) WAT and liver in *LysM-Cre Sucnr1*^{fl/fl} mice than in *Sucnr1*^{fl/fl} mice (Fig. 1f), whereas *Arg1*, *Mrc1*, *Fizz1* (also known as *Retnla*), *Il10*, *Il4ra* and *Il1rn* were downregulated, particularly in the scWAT (Fig. 1g).

We next assessed the timing of glucose intolerance and insulin sensitivity in *LysM-Cre Sucnr1*^{fl/fl} mice. Insulin resistance, but not glucose intolerance, was detected in 15-week-old *LysM-Cre Sucnr1*^{fl/fl} mice, but not in *Sucnr1*^{fl/fl} mice (Supplementary Fig. 2d). WAT and liver inflammation, as assessed by expression of pro-inflammatory genes (*Il1b*, *Il6*, *Il12b*, *Tnf* and *Nos2*), was manifest at 12 weeks of age in *LysM-Cre Sucnr1*^{fl/fl} mice (Supplementary Fig. 2e), at a time when glucose tolerance and insulin sensitivity were still similar to *Sucnr1*^{fl/fl} control mice (Supplementary Fig. 2d), suggesting that in this model inflammation precedes the induction of insulin resistance.

Mirroring the increase in adipose-tissue inflammation, the number of CD11b⁺F4/80⁺ macrophages in the stromal vascular fraction (SVF) of scWAT and vWAT (referred to as ATMs hereafter) was significantly higher in *LysM-Cre Sucnr1*^{fl/fl} than in *Sucnr1*^{fl/fl} mice, as measured by flow cytometry (Fig. 1h). The percentage

of SVF CD11b⁺ myeloid cells in the scWAT and vWAT were similar in *LysM-Cre Sucnr1*^{fl/fl} and *Sucnr1*^{fl/fl} mice (Supplementary Fig. 2f) and there were no significant differences in the number of CD11b⁺Ly6G⁺ neutrophils (Supplementary Fig. 2g). Sorting of CD11b⁺CD11c⁺CD206⁻ pro-inflammatory macrophages and CD11b⁺CD11c⁻CD206⁺ anti-inflammatory macrophages²⁶ from the scWAT indicated a significant increase in the percentage of CD11b⁺CD11c⁺CD206⁻ macrophages in *LysM-Cre Sucnr1*^{fl/fl} (25.9%) compared with *Sucnr1*^{fl/fl} mice (18.8%), concomitant with a decrease in the percentage of CD11b⁺CD11c⁻CD206⁺ macrophages (0.8%) in *LysM-Cre Sucnr1*^{fl/fl} mice compared with *Sucnr1*^{fl/fl} mice (1.3%; Supplementary Fig. 2h). In addition, immunoblot analysis of mitogen-activated protein kinase JNK phosphorylation in adipose tissue²⁷ indicated JNK activation in the scWAT and vWAT of *LysM-Cre Sucnr1*^{fl/fl} mice relative to *Sucnr1*^{fl/fl} mice (Fig. 1i). These results suggested that myeloid-specific deficiency of *Sucnr1* promoted an overt pro-inflammatory response and disrupted glucose homeostasis during steady state.

Myeloid *Sucnr1* deficiency exacerbates diet-induced obesity.

We next assessed the susceptibility of *LysM-Cre Sucnr1*^{fl/fl} mice to high-fat diet (HFD)-induced obesity. Body-weight gain was significantly increased in HFD *LysM-Cre Sucnr1*^{fl/fl} mice relative to HFD *Sucnr1*^{fl/fl} mice (Fig. 2a and Supplementary Fig. 3a), which correlated with a significant increase in the mass of the WAT, pancreas and liver (Supplementary Fig. 3b). Plasma levels of succinate were significantly higher in *LysM-Cre Sucnr1*^{fl/fl} mice than in *Sucnr1*^{fl/fl} mice (Fig. 2b). Also, intracellular succinate was higher in WAT (Supplementary Fig. 3c), adipocytes and ATMs isolated from fat depots (Supplementary Fig. 3d) of *LysM-Cre Sucnr1*^{fl/fl} than of *Sucnr1*^{fl/fl} mice. Expression of *Sucnr1* mRNA in scWAT was higher in HFD *LysM-Cre Sucnr1*^{fl/fl} and HFD *Sucnr1*^{fl/fl} mice than in NCD mice of both genotypes (Fig. 2b), whereas HFD decreased the expression of *Sucnr1* mRNA in ATMs from scWAT of *Sucnr1*^{fl/fl} mice

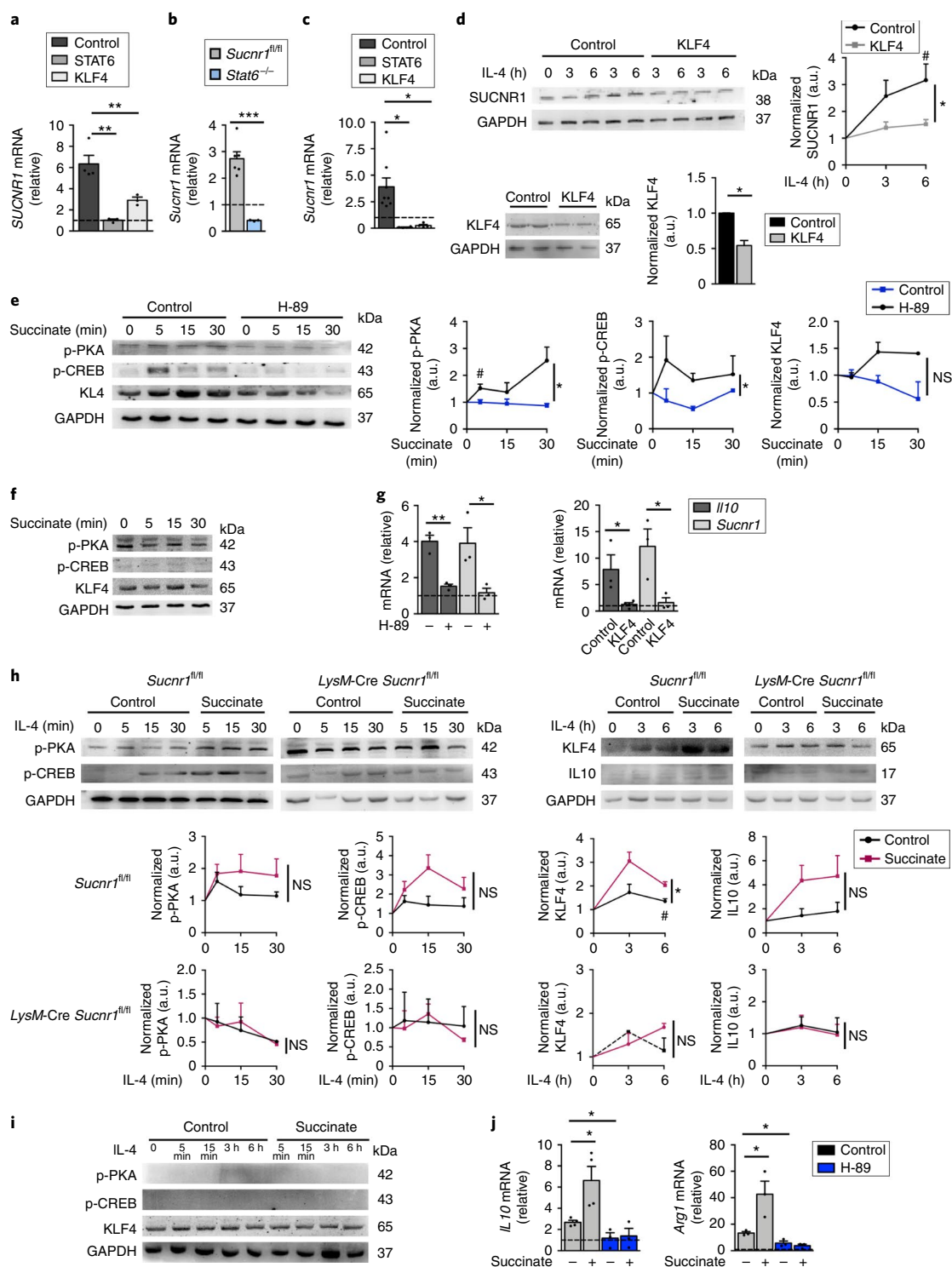


Fig. 4 | SUCNR1 signaling in macrophages. **a**, SUCNR1 mRNA in THP1 cells transfected with siRNAs (control, STAT6 and KLF4) and stimulated with IL-4 for 6 h (control, $n = 4$; STAT6 and KLF4, $n = 3$). **b**, **c**, qPCR analysis of expression of *Sucnr1* in *Sucnr1^{fl/fl}* BMDMs ($n = 6$) and *Stat6^{-/-}* BMDMs ($n = 3$) (**b**) and *Sucnr1^{fl/fl}* BMDMs transfected with siRNAs for STAT6 ($n = 4$), KLF4 ($n = 4$) or control vector ($n = 8$) (**c**) after stimulation with IL-4. **d**–**f**, Immunoblot analysis of selected proteins in *Sucnr1^{fl/fl}* BMDMs transfected with control and KLF4 siRNAs (**d**), *Sucnr1^{fl/fl}* BMDMs pretreated with H-89 for 30 min (**e**) and *LysM-Cre Sucnr1^{fl/fl}* BMDMs stimulated with succinate (**f**). **g**, qPCR analysis of selected genes in *Sucnr1^{fl/fl}* BMDMs pretreated with H-89 or transfected with siRNA KLF4 after succinate stimulation for 6 h ($n = 3$ per group, except $n = 4$ for *Il10* mRNA in KLF4 with succinate). **h**, **i**, Immunoblot analysis of *LysM-Cre Sucnr1^{fl/fl}* and *Sucnr1^{fl/fl}* BMDMs pre-incubated with succinate for 2 h (**h**) and *Sucnr1^{fl/fl}* BMDMs treated with H-89 and pre-incubated with succinate (**i**). **j**, Expression of *Il10* and *Arg1* in *Sucnr1^{fl/fl}* BMDMs pretreated with succinate and H-89 ($n = 3$ and $n = 4$ for *Il10* mRNA in control without H-89). Results are represented relative to respective basal expression as 1 (without IL-4 in **a**–**c**; without succinate stimulation in **g**). **d**, **e**, **f**, **h**, **i**, Representative image and densitometry analysis. **a**–**j**, n represents biologically independent samples. **a**–**c**, **g**, **j**, Values are expressed as mean \pm s.e.m.; * $P < 0.05$; ** $P < 0.01$; *** $P < 0.001$ (two-tailed unpaired t -test). **d**, **e**, **h**, Values are expressed as mean \pm s.e.m.; # $P < 0.05$ versus time 0; * $P < 0.05$ versus control; NS, non-significant (two-tailed paired t -test). For immunoblots, GAPDH was used as the loading control. Uncropped blots are provided in source data.

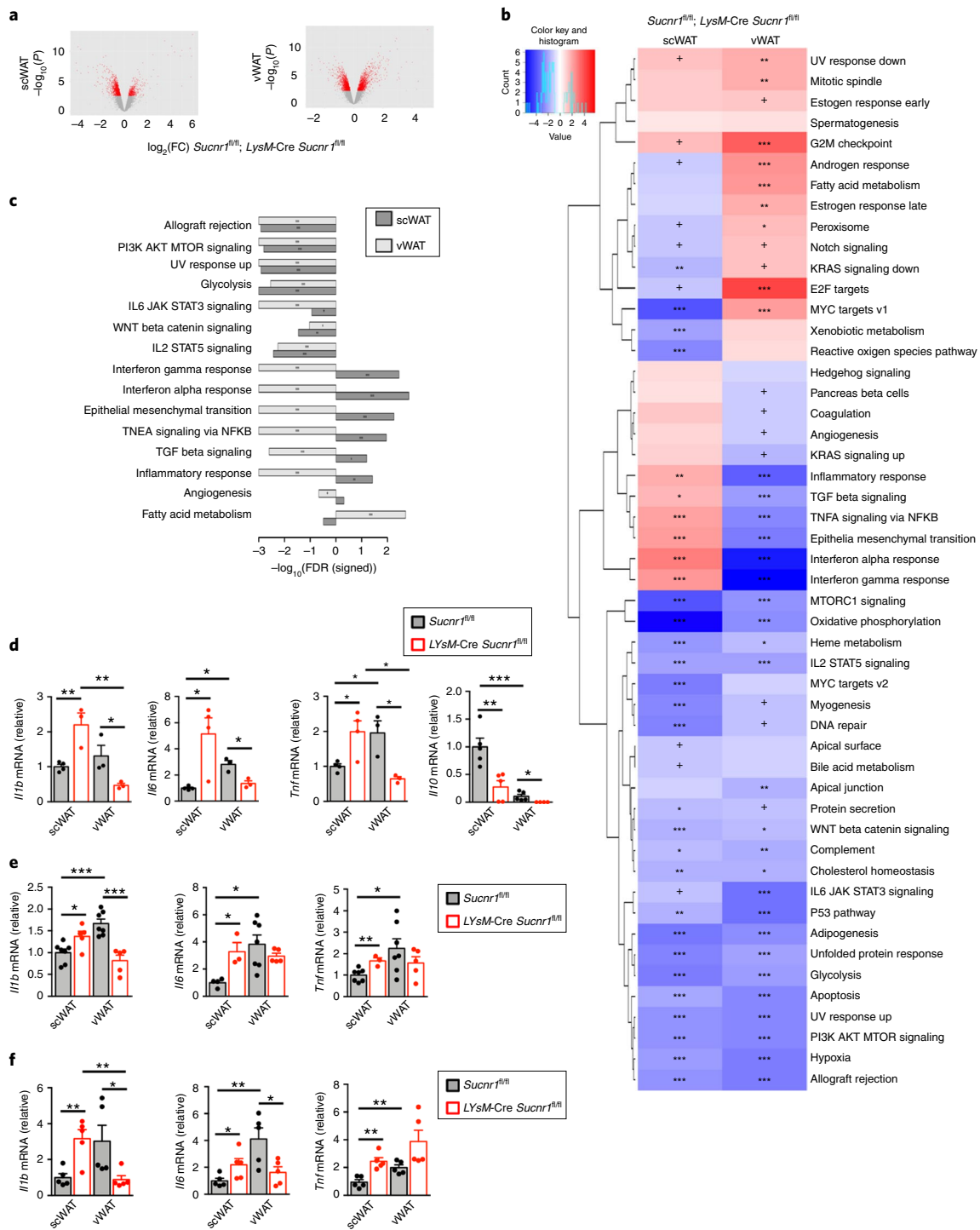


Fig. 5 | *LysM-Cre Sucnr1^{fl/fl}*-deficient ATMs show an altered transcriptome signature. **a**, Volcano plots for microarray gene expression of scWAT and vWAT ATMs from *LysM-Cre Sucnr1^{fl/fl}* and *Sucnr1^{fl/fl}* mice. Linear models with empirical Bayes statistic (Limma) were used for differential expression. Genes in red have Benjamini-Hochberg adjusted $P < 0.05$. **b**, Heat map with GSEA normalized enrichment scores (and significance) for ATMs as in **a** on Hallmark gene sets. P values were calculated by gene set permutations. False discovery rates (FDR) are indicated by symbols in each cell: +, *, ** and *** for 0.25, 0.10, 0.05 and 0.01, respectively. **c**, Bar plots showing enrichment scores ($-\log_{10}$ of FDR P values (signed)) of Hallmarks (GSEA) distinguishing between downregulated (shown in negative) and upregulated (shown in positive) pathways (filtered by gene sets with FDR < 0.25) for ATMs as in **a**. **a-c**, $n = 4$ biologically independent samples. **d-f**, qPCR analysis of selected genes in ATMs (**d**) and $\text{Cd11b}^+\text{CD11c}^+\text{CD206}^-$ (**e**) and $\text{Cd11b}^+\text{CD11c}^-\text{CD206}^+$ (**f**) cell populations from ATMs as in **a** (**d**, $n = 4$ or 3; **e**, $n = 7$ or 5; and **f**, $n = 5$ for *Sucnr1^{fl/fl}* or *LysM-Cre Sucnr1^{fl/fl}*, respectively; biologically independent samples). Data are expressed as mean \pm s.e.m.; * $P < 0.05$; ** $P < 0.01$; *** $P < 0.001$ (two-tailed unpaired t -test).

(Fig. 2b). This suggested that the increased expression of *Sucnr1* mRNA in the scWAT in HFD *LysM-Cre Sucnr1^{fl/fl}* and *Sucnr1^{fl/fl}* mice originated from mature adipocytes.

The size of adipocytes in the scWAT of HFD *LysM-Cre Sucnr1^{fl/fl}* mice was significantly increased compared with *Sucnr1^{fl/fl}* mice (Supplementary Fig. 3e). There was also an increase in the number

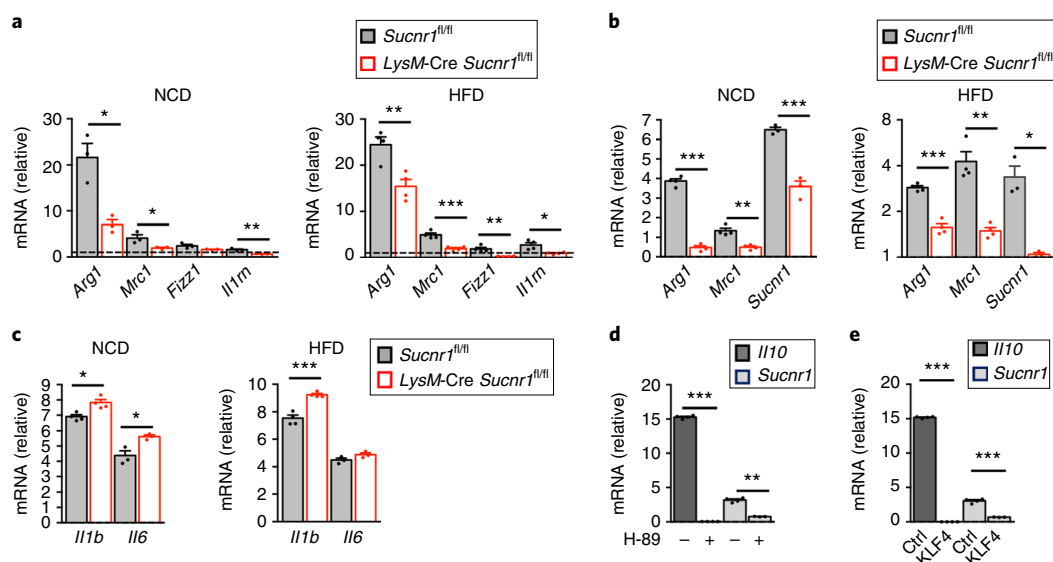


Fig. 6 | *Sucnr1*-deficient subcutaneous ATMs are unresponsive to IL-4 and succinate. **a**, qPCR analysis of selected genes in scWAT ATMs from *Sucnr1^{fl/fl}* and *LysM-Cre Sucnr1^{fl/fl}* mice fed a NCD or HFD stimulated with IL-4 for 6 h ($n=3$ for NCD and $n=4$ for HFD, except $n=3$ in *Il1rn* mRNA in *Sucnr1^{fl/fl}*). **b**, qPCR analysis of selected genes as in **a** stimulated with succinate for 6 h ($n=4$, except $n=3$ for *Sucnr1* mRNA). **c**, qPCR analysis of selected genes as in **a** stimulated with LPS for 6 h ($n=4$, except $n=3$ for *Il6* mRNA). **d**, qPCR analysis of gene expression of *Il10* and *Sucnr1* in scWAT ATMs on a NCD, pretreated or not with H-89 (30 min) before stimulation with succinate for 6 h ($n=4$, except $n=3$ for *Sucnr1* mRNA in H-89). **e**, qPCR analysis of gene expression of *Il10* and *Sucnr1* as in **d**, transfected with siRNA against KLF4 or control before stimulation with succinate for 6 h ($n=4$, except $n=3$ for *Sucnr1* mRNA in KLF4). Results are presented relative to their respective basal expression as 1 (without IL-4 in **a**, without succinate in **b**, **d** and **e**) and without LPS in **c**. **a–e**, n represents biologically independent samples. Values are expressed as mean \pm s.e.m., in **b–e** data are \log_2 (value + 1) transformed; * $P < 0.05$; ** $P < 0.01$; *** $P < 0.001$ (two-tailed unpaired t -test).

of crown-like structures in the scWAT and vWAT of HFD *LysM-Cre Sucnr1^{fl/fl}* mice compared with control mice (Fig. 2c). Of note, the increased weight gain in HFD *LysM-Cre Sucnr1^{fl/fl}* mice was not associated with changes in food intake compared with HFD *Sucnr1^{fl/fl}* mice (Supplementary Fig. 3f). Indirect calorimetry showed similar oxygen consumption and carbon dioxide production in both genotypes (Supplementary Fig. 3g). Likewise, there were no significant differences in energy expenditure (Fig. 2d). When the data were corrected to body weight, analysis of covariance²⁸ indicated that the differences detected in energy expenditure were genotype dependent (Supplementary Fig. 3h). The lower respiratory exchange ratio (VCO_2/VO_2) in HFD *LysM-Cre Sucnr1^{fl/fl}* compared with HFD *Sucnr1^{fl/fl}* mice (Fig. 2d) indicated a preference in these mice to metabolize fat as energy²⁹.

HFD *LysM-Cre Sucnr1^{fl/fl}* mice had a higher fasting hyperglycemia and hyperinsulinemia than HFD *Sucnr1^{fl/fl}* mice (Fig. 2e). Consistently, HFD *LysM-Cre Sucnr1^{fl/fl}* mice showed impaired glucose tolerance (Fig. 2f) and insulin sensitivity (Fig. 2g) relative to HFD *Sucnr1^{fl/fl}* mice. No significant differences in glucose tolerance and insulin sensitivity were detected between both genotypes before their body weight diverged (11–15 weeks of age) (Supplementary Fig. 3i), indicating that the loss of glucose homeostasis in HFD *LysM-Cre Sucnr1^{fl/fl}* mice was linked to their obese phenotype. Further, no significant differences in oxygen consumption, carbon dioxide production and energy expenditure were detected between genotypes at 14 weeks of age (Supplementary Fig. 3j), indicating that, in response to dietary excess, the metabolic differences between both genotypes were mostly related to weight gain.

Similarly to the findings on NCD, HFD *LysM-Cre Sucnr1^{fl/fl}* mice showed higher expression of several pro-inflammatory markers (*Il12b*, *Tnf* and *Nos2*) in WAT and liver (Fig. 2h) and a decrease in the expression of some anti-inflammatory markers (*Arg1*, *Mrc1*, *Il10* and *Il4ra*) in scWAT (Fig. 2i) compared with HFD *Sucnr1^{fl/fl}* mice. We observed a higher frequency of CD11b⁺CD11c⁺CD206⁻

pro-inflammatory macrophages (23.8%), along with a trend for a lower frequency of CD11b⁺CD11c⁻CD206⁺ anti-inflammatory macrophages (1.3%) in the scWAT of HFD *LysM-Cre Sucnr1^{fl/fl}* compared with HFD *Sucnr1^{fl/fl}* mice (19.3 and 3.1%, respectively) (Supplementary Fig. 3k). Taken together, the results indicate that myeloid-specific *Sucnr1* deficiency increases the susceptibility to diet-induced obesity.

***Sucnr1* signaling regulates cell-autonomous macrophage polarization.**

To address whether intracellular and extracellular succinate had different effects on macrophages, first we investigated whether expression of *Sucnr1* mRNA was affected by the activation status of macrophages. As reported before^{3,23,24}, stimulation with LPS, but not interleukin-4 (IL-4), increased the secretion of succinate in peritoneal macrophages in vitro (Fig. 3a), and correlated with an accumulation of intracellular succinate (Supplementary Fig. 4a), as previously described³⁰. Expression of *Sucnr1* mRNA in peritoneal macrophages was robustly increased by IL-4 and strongly decreased by LPS (Fig. 3a), while *SUCNR1* mRNA in the human monocytic-like cell line THP1 was induced by macrophage colony-stimulating factor (M-CSF) and decreased by granulocyte macrophage colony-stimulating factor (GM-CSF) (Supplementary Fig. 4b). In macrophages differentiated with GM-CSF from human peripheral blood mononuclear cells (hPBMCs), succinate secretion was increased compared with non-differentiated (control) cells, whereas *SUCNR1* mRNA was increased in macrophages differentiated with M-CSF compared with control cells (Fig. 3b). Polarization of hPBMC macrophages by GM-CSF or M-CSF was confirmed by measuring the expression of pro-inflammatory-associated (*Il1b*, *Il6*, *Il12b*, *Tnf* and *Mcp1*) and anti-inflammatory-associated (*PPAR γ* and *Mrc1*) genes, respectively³¹ (Supplementary Fig. 4c). Macrophages derived from hPBMCs and differentiated with M-CSF (hereafter hPBMC^{M-CSF} macrophages) can be polarized towards a pro- or an anti-inflammatory phenotype with the appropriate exogenous stimuli³². LPS

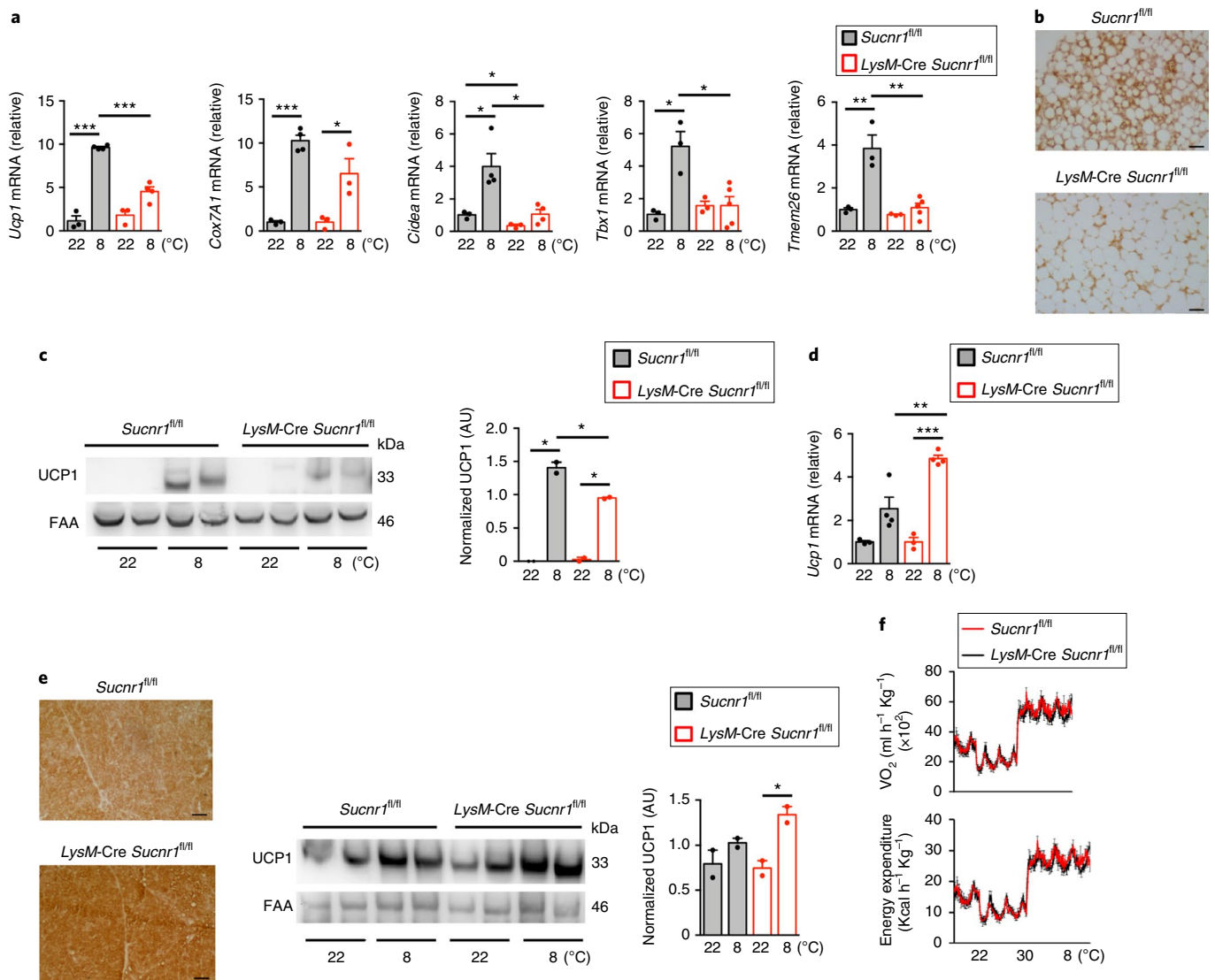


Fig. 7 | *LysM-Cre Sucnr1^{fl/fl}* mice are refractory to prolonged cold-induced browning in scWAT. **a, qPCR analysis of *Ucp1* and typical markers of beige activation in scWAT from male *Sucnr1^{fl/fl}* and *LysM-Cre Sucnr1^{fl/fl}* mice housed at 8 °C or 22 °C for 6 d ($n=3$ mice at 22 °C; $n=4$ for *Sucnr1^{fl/fl}* and $n=5$ for *LysM-Cre Sucnr1^{fl/fl}* at 8 °C). Results are transformed as $\log_2(\text{value} + 1)$ normalized to gene expression of *Sucnr1^{fl/fl}* mice at 22 °C. **b**, Representative images of immunohistochemical staining of UCP1 in scWAT as in **a** housed at 8 °C, from two independent experiments ($n=4$ mice). Scale bars, 200 μm . **c**, Representative images of immunoblot analysis of UCP1 in scWAT (left) as in **a** and quantification performed as the ratio of UCP1/FAA presented in arbitrary units (right) ($n=2$ mice). **d**, qPCR analysis of *Ucp1* in BAT as in **a** ($n=3$ per genotype at 22 °C and $n=4$ per genotype at 8 °C). **e**, Representative images of immunohistochemical staining of UCP1 in BAT from two independent experiments (left, $n=4$ mice) and immunoblot analysis of UCP1 protein in BAT (middle) and quantification (right) performed as the ratio of UCP1/FAA presented in arbitrary units ($n=2$ mice). Scale bars, 200 μm . Representative results from two independent experiments with similar results. Uncropped blots are provided in source data. **f**, Energy expenditure and oxygen consumption (VO_2) of *Sucnr1^{fl/fl}* and *LysM-Cre Sucnr1^{fl/fl}* mice acutely subjected to 8 °C from thermoneutrality (30 °C). Data are shown as mean \pm s.e.m.; * $P < 0.05$; ** $P < 0.01$; *** $P < 0.001$ (two-tailed unpaired *t*-test).**

significantly decreased the expression of *SUCNR1* mRNA in macrophages derived from hPBMCs and differentiated with M-CSF, whereas IL-4 strongly enhanced its expression (Fig. 3c). Accordingly, the expression of anti-inflammatory markers, such as *Arg1* and *Fizz1*, and fatty acid metabolic genes, such as *Cpt1a* and *Fasn*, was significantly lower in peritoneal macrophages isolated from *LysM-Cre Sucnr1^{fl/fl}* compared with those isolated from *Sucnr1^{fl/fl}* mice (Fig. 3d). We detected a lower expression of *Arg1* and *Mrc1* in IL-4-treated *LysM-Cre Sucnr1^{fl/fl}* peritoneal macrophages compared with IL-4-treated *Sucnr1^{fl/fl}* peritoneal macrophages (Fig. 3e). M-CSF-treated BMDMs (hereafter BMDMs^{M-CSF}) from *LysM-Cre Sucnr1^{fl/fl}* mice also expressed less anti-inflammatory genes (*Arg1*, *Mrc1* and *Fizz1*) compared with *Sucnr1^{fl/fl}* BMDMs^{M-CSF} (Fig. 3f). M-CSF, but

not GM-CSF, induced the expression of *Sucnr1* mRNA in BMDMs (Supplementary Fig. 4d). Accordingly, succinate enhanced the expression *Arg1*, *Mrc1*, *Fizz1* and *Il10* in *Sucnr1^{fl/fl}* BMDMs^{M-CSF}, but not in *LysM-Cre Sucnr1^{fl/fl}* BMDMs^{M-CSF} (Fig. 3g). Addition of succinate to *Sucnr1^{fl/fl}* BMDMs^{M-CSF} did not increase the amount of intracellular succinate, whereas the cell-permeable dimethyl succinate did (Supplementary Fig. 4e). There were no significant differences in the amount of intracellular succinate between *Sucnr1^{fl/fl}* BMDMs and *LysM-Cre Sucnr1^{fl/fl}* BMDMs (Supplementary Fig. 4f).

An *in silico* analysis of the *Sucnr1* promoter region in BMDMs revealed binding sites for the IL-4-responsive transcription factor STAT6 (Supplementary Fig. 5a). To test whether expression of *SUCNR1* in macrophages was regulated by IL-4, we used short

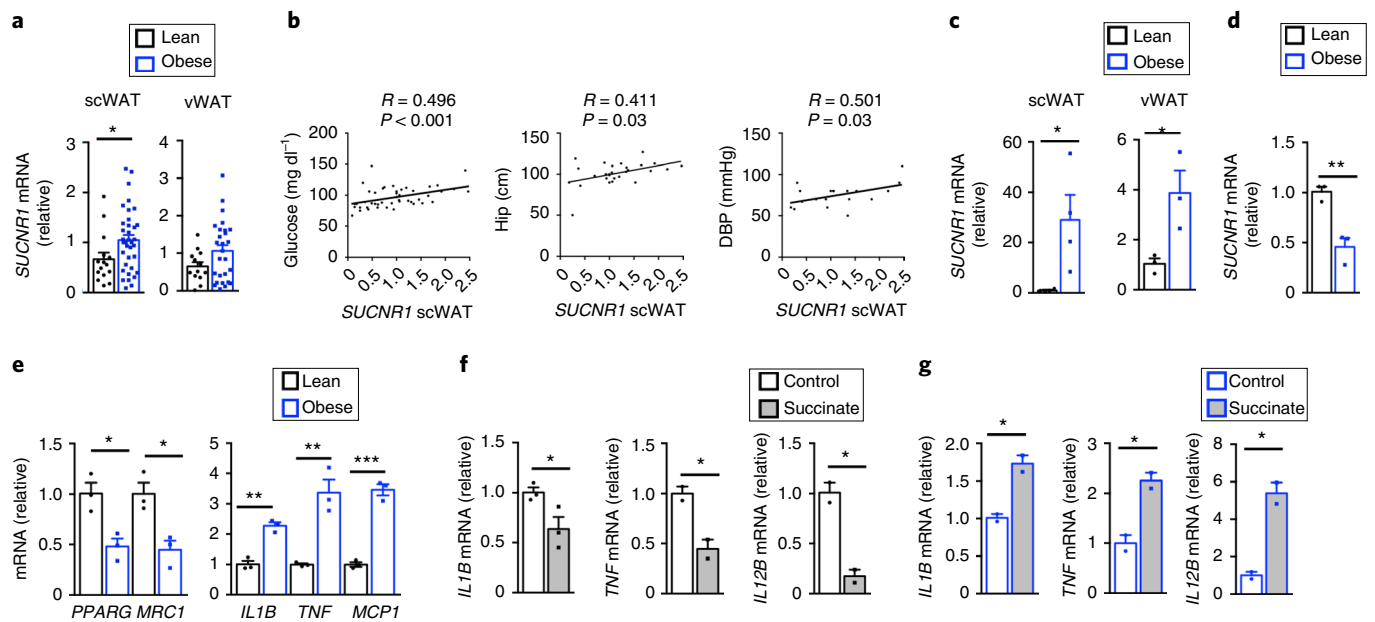


Fig. 8 | Obese human adipose tissue is insensitive to the anti-inflammatory effects of succinate. **a**, qPCR analysis of expression of *SUCNR1* in scWAT and vWAT from human lean ($n=15$ for scWAT and $n=13$ for vWAT) and obese ($n=36$ for scWAT and $n=27$ for vWAT) patients. **b**, Correlation between *SUCNR1* gene expression in scWAT with glucose ($n=46$), hip circumference ($n=28$) and diastolic blood pressure (DBP) ($n=19$) from human patients. **c**, **d**, qPCR analysis of expression of *SUCNR1* in subcutaneous adipocytes (scAD) or visceral adipocytes (vAD) (**c**) and scWAT ATMs (**d**) from lean and obese patients ($n=4$, $n=3$ and $n=3$). **e**, qPCR analysis of selected genes in human scWAT ATMs ($n=3$). **f**, **g**, qPCR analysis of pro-inflammatory genes in human scWAT explants, unstimulated or stimulated with succinate for 24 h, from lean (**f**) and obese (**g**) patients ($n=2$ and $n=3$ for expression of *IL1B*, *TNF* and *IL12B* in scWAT derived from a pool of three patients per phenotype). **a–g**, n represents biologically independent samples. Results are expressed as mean \pm s.e.m.; * $P < 0.05$; ** $P < 0.01$; *** $P < 0.001$ (two-tailed unpaired t -test). For **b** Spearman's (in glucose and HIP graph) or Pearson's (in diastolic blood pressure graph) correlation analysis was used.

interfering RNA (siRNA) to knock down the expression of STAT6 or KLF4, a transcription factor whose expression is induced by STAT6 in macrophages³³. The IL-4-induced expression of *IL10*, *PPARG* and *IL1RN* (Supplementary Fig. 5b) and *SUCNR1* (Fig. 4a) was lower in THP1 cells in which STAT6 or KLF4 were knocked down compared with control-siRNA-treated THP1 macrophages (65% or 68% efficiency of knockdown, respectively). IL-4 stimulation upregulated *Sucnr1* (Fig. 4b) and *Arg1*, *Mrc1* and *Il10* mRNA (Supplementary Fig. 5c) in *Sucnr1*^{fl/fl} BMDMs^{M-CSF}, but not in *Stat6*^{-/-} BMDMs^{M-CSF}. Knockdown of STAT6 and KLF4 also decreased the upregulation of *Sucnr1* (Fig. 4c) and *Arg1*, *Mrc1* and *Il10* mRNA (Supplementary Fig. 5d) in response to IL-4 in *Sucnr1*^{fl/fl} BMDMs^{M-CSF}. Knockdown of KLF4 in BMDMs^{M-CSF} also decreased the IL-4-induced expression of *SUCNR1* protein (Fig. 4d), while IL-4 did not upregulate expression of KLF4 or *SUCNR1* protein in *Stat6*^{-/-} BMDMs^{M-CSF} (Supplementary Fig. 5e).

The KLF4 promoter contains cyclic AMP response element-binding protein (CREB)-binding sites³⁴ and can therefore be modulated by G protein-coupled receptor ligands, which can act synergically with IL-4 through the activation of the cyclic AMP-CREB pathway^{34,35}. Consistent with this notion, short-term exposure of *Sucnr1*^{fl/fl} BMDMs^{M-CSF} to succinate induced the phosphorylation of protein kinase A (PKA) and CREB, which was blocked by the PKA inhibitor H-89 (Fig. 4e). The succinate-mediated activation of the PKA-CREB pathway was not detected in *LysM-Cre Sucnr1*^{fl/fl} BMDMs^{M-CSF} (Fig. 4f), while H-89-mediated inhibition of PKA or knockdown of *Klf4* by siRNA in *Sucnr1*^{fl/fl} BMDMs^{M-CSF} suppressed the induction of *Il10* and *Sucnr1* mRNA by succinate (Fig. 4g). Finally, we assessed the effect of succinate on IL-4 signaling. Whereas succinate treatment did not significantly modify the IL-4-induced activation of STAT6 in *Sucnr1*^{fl/fl} BMDMs^{M-CSF} (Supplementary Fig. 5f), succinate increased the IL-4-induced

activation of PKA and CREB in these cells, an effect that was absent in *LysM-Cre Sucnr1*^{fl/fl} BMDMs^{M-CSF} (Fig. 4h) and abolished by H-89 treatment (Fig. 4i). Succinate increased the IL-4-induced expression of KLF4 and IL-10 in *Sucnr1*^{fl/fl} BMDMs^{M-CSF}, but not in *LysM-Cre Sucnr1*^{fl/fl} BMDMs^{M-CSF} (Fig. 4h), suggesting that succinate enhanced IL-4 signaling by modulating the activation of PKA and CREB and the expression of KLF4. Accordingly, addition of H-89 prevented the succinate-induced increase in *Il10* and *Arg1* mRNA in IL-4-treated BMDMs^{M-CSF} (Fig. 4j). Overall, these data indicated that succinate-SUCNR1 signaling promoted an anti-inflammatory phenotype in macrophages.

***Sucnr1* deficiency alters intracellular signaling in ATMs.** Because ATMs play key roles in obesity-induced inflammation³⁶, we performed transcriptomic analysis on ATMs sorted from the scWAT and vWAT of *LysM-Cre Sucnr1*^{fl/fl} and *Sucnr1*^{fl/fl} mice. Genes (242 total, 85 upregulated, 157 downregulated) were differentially expressed in scWAT ATMs, and 271 genes (174 upregulated, 97 downregulated) were differentially expressed in vWAT ATMs (fold change > 2 , adjusted $P < 0.05$) from *LysM-Cre Sucnr1*^{fl/fl} mice compared with *Sucnr1*^{fl/fl} mice (Fig. 5a). Gene set enrichment analysis (GSEA) indicated that loss of *Sucnr1* resulted in altered gene expression patterns in vWAT ATMs compared with scWAT ATMs (Fig. 5b). Specifically, inflammatory pathways such as interferon, epithelial mesenchymal transition and tumor necrosis factor (TNF) response were upregulated in *LysM-Cre Sucnr1*^{fl/fl} compared with *Sucnr1*^{fl/fl} scWAT ATMs, while they were downregulated in *LysM-Cre Sucnr1*^{fl/fl} compared with *Sucnr1*^{fl/fl} vWAT ATMs (Fig. 5c). The opposite outcomes of *Sucnr1* deficiency in the transcriptional signature of ATMs (Fig. 5c and Supplementary Fig. 6a,b) were associated to the pro-inflammatory profile of *Sucnr1*^{fl/fl} vWAT ATMs compared with *Sucnr1*^{fl/fl} scWAT ATMs (Supplementary Fig. 6a,b), previously

described in vWAT compared with scWAT³⁷. GSEA analysis of the genes differentially regulated between scWAT ATMs and vWAT ATMs indicated the upregulation of inflammatory pathways in *LysM-Cre Sucnr1^{fl/fl}* vWAT ATMs compared with *LysM-Cre Sucnr1^{fl/fl}* scWAT ATMs (Supplementary Fig. 7a,b and Supplementary Tables 1 and 2). Independent validation by quantitative PCR (qPCR) indicated increased expression of *Il1b*, *Il6* and *Tnf* and decreased expression of *Il10* in *LysM-Cre Sucnr1^{fl/fl}* scWAT ATMs compared with *Sucnr1^{fl/fl}* scWAT ATMs (Fig. 5d). A decrease in *Tnf* and *Il10* mRNA was observed in *LysM-Cre Sucnr1^{fl/fl}* vWAT ATMs compared with *Sucnr1^{fl/fl}* vWAT ATMs (Fig. 5d). Both CD11b⁺CD11c⁺CD206⁻ pro-inflammatory and CD11b⁺CD11c⁻CD206⁺ anti-inflammatory macrophages from the *LysM-Cre Sucnr1^{fl/fl}* scWAT (but not the vWAT) showed increased expression of pro-inflammatory genes compared with CD11b⁺CD11c⁺CD206⁻ and CD11b⁺CD11c⁻CD206⁺ macrophages from *Sucnr1^{fl/fl}* mice (Fig. 5e,f).

The IL-4- and succinate-induced expression of anti-inflammatory markers (*Arg1*, *Mrc1*, *Fizz1* and *Il1rn*) was lower in *LysM-Cre Sucnr1^{fl/fl}* than in *Sucnr1^{fl/fl}* scWAT ATMs, both in cells isolated from mice fed a NCD or HFD (Fig. 6a,b). By contrast, LPS induction of *Il1b* mRNA was higher in *LysM-Cre Sucnr1^{fl/fl}* than in *Sucnr1^{fl/fl}* scWAT ATMs, in cells isolated from mice fed a NCD or HFD (Fig. 6c). Moreover, the succinate-induced expression of *Il10* and *Sucnr1* was blocked by inhibition of PKA (Fig. 6d) or knockdown of KLF4 (Fig. 6e) in scWAT ATMs from *Sucnr1^{fl/fl}* mice. Thus, signaling through SUCNR1 had both inflammatory²³ and anti-inflammatory program in scATMs.

Myeloid *Sucnr1* deficiency impairs cold-induced browning of scWAT. Type 2 immune signaling regulates adipose thermogenesis^{38–40}. Next, we investigated whether succinate–SUCNR1 signaling in macrophages was involved in beige cell activation in the scWAT and cold-induced thermogenesis. Prolonged cold exposure (8 °C for 6 d) led to a marked induction of *Ucp1* and other key thermogenic genes in the scWAT of *Sucnr1^{fl/fl}* mice, but only to poor induction in the scWAT of *LysM-Cre Sucnr1^{fl/fl}* mice (Fig. 7a). Immunohistochemical analysis of scWAT indicated the formation of multilocular, brown-like adipocytes in *Sucnr1^{fl/fl}* mice following cold exposure, but this effect was noticeably reduced in *LysM-Cre Sucnr1^{fl/fl}* mice (Fig. 7b). Immunoblotting indicated a marked impairment in the cold-induced expression of *Ucp1* protein in the scWAT of *LysM-Cre Sucnr1^{fl/fl}* compared with *Sucnr1^{fl/fl}* mice (Fig. 7c). However, the interscapular brown adipose tissue (BAT) of *LysM-Cre Sucnr1^{fl/fl}* mice had higher *Ucp1* expression, both mRNA (Fig. 7d) and protein (Fig. 7e), following prolonged cold exposure compared with the interscapular BAT of *Sucnr1^{fl/fl}* mice. No significant differences were detected in energy expenditure or whole-body oxygen consumption in *LysM-Cre Sucnr1^{fl/fl}* and *Sucnr1^{fl/fl}* mice housed at ambient temperature (22 °C), thermoneutrality (30 °C) or prolonged cold exposure (Fig. 7f). These results indicate that loss of *Sucnr1* in myeloid cells limited the browning of scWAT, which is considered a type 2 immune response⁴⁰.

Obesity disturbs succinate–SUCNR1 signaling in human adipose tissue. Circulating levels of succinate are higher in obese than in lean humans¹¹. To determine whether obesity impacts SUCNR1 function in human adipose tissues, we analyzed its expression in scWAT and vWAT biopsies from people classified according to body mass index (BMI) (Supplementary Table 3). Circulating levels of succinate were higher in obese subjects than in lean controls (Supplementary Table 3)¹¹. Further, expression of *SUCNR1* mRNA was higher in WAT from obese subjects than from lean ones, particularly in scWAT (Fig. 8a). Notably, we found a positive association between expression of *SUCNR1* in scWAT and clinical parameters associated with an altered metabolic profile such as blood glucose, hip

circumference and diastolic blood pressure (Fig. 8b). Cellular fractionation of scWAT biopsies indicated increased expression of *SUCNR1* in mature adipocytes in obese subjects compared with lean (Fig. 8c), whereas the opposite was seen in scWAT ATMs (Fig. 8d). The decrease in *SUCNR1* mRNA in scWAT ATMs from obese compared with lean subjects correlated with lower *PPARG* and *MRC1* mRNA expression and was concomitant with higher expression of the pro-inflammatory genes *IL1B*, *TNF* and *MCPI* (Fig. 8e). To examine the effects of extracellular succinate in the adipose tissue with respect to inflammation, we incubated WAT explants obtained from lean and obese subjects with succinate for 24 h. Incubation of lean-derived scWAT with succinate significantly decreased the expression of the pro-inflammatory cytokines *IL1B*, *TNF* and *IL12B* compared with non-stimulated scWAT (Fig. 8f). By contrast, succinate increased mRNA expression of *IL1B*, *TNF* and *IL12B* in vWAT compared with non-stimulated vWAT (Fig. 8g). These observations suggest that succinate–SUCNR1 signaling had an anti-inflammatory role in the human scWAT, which was disturbed in obesity.

Discussion

Here we show that loss of succinate-mediated signaling through SUCNR1 in myeloid cells impaired the induction of an anti-inflammatory program in macrophages and the response to type 2 cytokines, including those associated with diet-induced obesity^{41,42} and long-term cold exposure^{38,40}. We showed that extracellular succinate acted in cooperation with IL-4 signaling through the activation of the PKA–CREB–KLF4 pathway and increased the IL-4 response in a cell-autonomous manner. Notably, *Sucnr1* deficiency altered the phenotype of ATMs in a manner dependent on the WAT localization, by promoting an inflammatory molecular signature in scWAT ATMs. Our results suggest a mechanism by which SUCNR1 signaling contributes to resolution of acute inflammation.

In response to metabolic and inflammatory challenge, succinate accumulates in pro-inflammatory macrophages^{20,43}, which triggers an inflammatory phenotype through activation of HIF-1 α ³. In this scenario, succinate is exported to the extracellular milieu²³ where it signals through SUCNR1^{2,23}. Though intracellular succinate is considered a pro-inflammatory stimulus^{2,3,23}, our observations indicated that SUCNR1 was mostly expressed in pro-resolving or anti-inflammatory macrophages, as previously reported⁴⁴. *LysM-Cre Sucnr1^{fl/fl}* mice developed local tissue inflammation and deregulated glucose homeostasis at steady state. Moreover, these mice showed higher susceptibility to development of diet-induced obesity compared with *Sucnr1^{fl/fl}* mice. *Sucnr1^{-/-}* mice have yielded contradictory results in terms of glucose homeostasis and susceptibility to develop obesity depending on HFD composition (45% versus 60% calories from fat)^{10,18}. Our results showed enhanced weight gain and impaired glucose tolerance in *LysM-Cre Sucnr1^{fl/fl}* compared with control mice in response to 45% HFD. This contrasts with the phenotype observed in the global *Sucnr1^{-/-}* mice fed with the same diet, in which there was a decrease of macrophage infiltration into adipose tissue and an improvement of glucose tolerance compared with control mice, despite similar increase in body weight¹⁰. These differences highlight the importance of cell-specific studies assessed by conditional knockout mouse models to adequately evaluate the role of SUCNR1 in individual cell subsets.

Our data indicated that extracellular succinate promoted an anti-inflammatory program in macrophages. BMDMs, peritoneal macrophages and scWAT ATMs from the *LysM-Cre Sucnr1^{fl/fl}* mice showed increased expression of pro-inflammatory markers (for example *Il1b*, *Il12b*, *Tnf* and *Nos2*) and did not upregulate expression of anti-inflammatory markers (for example *Arg1*, *Mrc1*, *Fizz1* and *Il10*) in response to IL-4, as observed in *Sucnr1^{fl/fl}* macrophages. This suggested that extracellular succinate triggered a pro-resolving phenotype in tissue-resident macrophages as ATMs, to counterbalance the inflammatory signals and recover metabolic homeostasis.

Consistent with this notion, succinate has been proposed to act as an 'alarmin' for the innate immune system, more specifically in dendritic cells^{3,22,23}. Anti-inflammatory properties for signaling through SUCNR1 have been previously reported. For example, inflammatory macrophage-derived succinate signals through SUCNR1 in neural stem cells to induce production of prostaglandin E2, triggering the resolution of inflammation during chronic neuroinflammation in mice with experimental autoimmune encephalomyelitis²⁴. Also, SUCNR1 signaling was reported as a potent activator of type 2 immunity and a surveillance mechanism for detection of certain helminths as *Tritrichomonas* in the small intestine of C57BL/6 mice²⁵. We propose a mechanism by which, like other signaling molecules such as IL-6^{45,46}, succinate is generated as part of an inflammatory program and acts as a negative feedback signal through SUCNR1 to promote an anti-inflammatory response in macrophages.

scWAT ATMs have a key role in metabolic homeostasis, and their remodeling is crucial to adequately respond to chronic positive energy balance^{47,48}. Our results indicated that in obese mice, loss of SUCNR1 in myeloid cells induced an inflammatory state in scWAT ATMs, but decreased the activation of inflammatory signaling pathways such as interferon and TNF response in vWAT ATMs. Comparative transcriptome profiling of ATMs from scWAT and vWAT from control mice revealed that vWAT ATMs were constitutively more inflamed than scWAT ATMs. This is consistent with the pro-inflammatory profile previously described in the visceral compared with the subcutaneous fat depots³⁷. Activation of SUCNR1 was reported to have a positive effect on the release of the pro-inflammatory cytokine IL-1 β in inflammatory macrophages. As such, during inflammation, succinate-SUCNR1 signaling may act as an anti-inflammatory mediator or boost inflammation²³ depending on the inflammatory status of cells expressing SUCNR1. Our data showed that activation of SUCNR1 decreased the expression of inflammatory-related genes in the scWAT of healthy subjects, whereas scWAT from obese patients was insensitive to signaling through SUCNR1. Extracellular succinate increased the expression of inflammatory markers in the scWAT from obese patients, which is known to shift towards a pro-inflammatory phenotype⁴⁹. Although obesity is characterized by high circulating amounts of succinate¹¹, ATMs from obese subjects had decreased expression of SUCNR1, along with other anti-inflammatory markers, such as PPAR γ and MRC1. This 'succinate-resistant state' in human obesity that might underlie, at least partially, the obesity-associated inflammation. The loss of this anti-inflammatory mechanism in obesity may contribute to the intrinsic inability of obese adipose tissue to resolve uncontrolled inflammation and to restore tissue homeostasis and functionality^{49,50}. As succinate-SUCNR1 signaling is emerging as a versatile and context-specific regulator of physiology and disease, further research is needed to provide a complete picture on its local and systemic modes of action.

Online content

Any methods, additional references, Nature Research reporting summaries, source data, statements of data availability and associated accession codes are available at <https://doi.org/10.1038/s41590-019-0372-7>.

Received: 2 March 2018; Accepted: 5 March 2019;

Published online: 08 April 2019

References

- Chouchani, E. T. et al. Ischaemic accumulation of succinate controls reperfusion injury through mitochondrial ROS. *Nature* **515**, 431–435 (2014).
- Rubic, T. et al. Triggering the succinate receptor GPR91 on dendritic cells enhances immunity. *Nat. Immunol.* **9**, 1261–1269 (2008).
- Tannahill, G. M. et al. Succinate is an inflammatory signal that induces IL-1 β through HIF-1 α . *Nature* **496**, 238–242 (2013).
- Toma, I. et al. Succinate receptor GPR91 provides a direct link between high glucose levels and renin release in murine and rabbit kidney. *J. Clin. Invest.* **118**, 2526–2534 (2008).
- Murphy, M. P. & O'Neill, L. A. J. Krebs cycle reimaged: the emerging roles of succinate and itaconate as signal transducers. *Cell* **174**, 780–784 (2018).
- Peti-Peterdi, J., Gevorgyan, H., Lam, L. & Riquier-Brison, A. Metabolic control of renin secretion. *Pflugers Arch.* **465**, 53–58 (2013).
- Hochachka, P. W. & Dressendorfer, R. H. Succinate accumulation in man during exercise. *Eur. J. Appl. Physiol. Occup. Physiol.* **35**, 235–242 (1976).
- Sadagopan, N. et al. Circulating succinate is elevated in rodent models of hypertension and metabolic disease. *Am. J. Hypertens.* **20**, 1209–1215 (2007).
- Aguiar, C. J. et al. Succinate causes pathological cardiomyocyte hypertrophy through GPR91 activation. *Cell Commun. Signal.* **12**, 78 (2014).
- van Diepen, J. A. et al. SUCNR1-mediated chemotaxis of macrophages aggravates obesity-induced inflammation and diabetes. *Diabetologia* **60**, 1304–1313 (2017).
- Serena, C. et al. Elevated circulating levels of succinate in human obesity are linked to specific gut microbiota. *ISME J.* **12**, 1642–1657 (2018).
- He, W. et al. Citric acid cycle intermediates as ligands for orphan G-protein-coupled receptors. *Nature* **429**, 188–193 (2004).
- Gilissen, J., Jouret, F., Piroette, B. & Hanson, J. Insight into SUCNR1 (GPR91) structure and function. *Pharmacol. Ther.* **159**, 56–65 (2016).
- de Castro Fonseca, M., Aguiar, C. J., da Rocha Franco, J. A., Gingold, R. N. & Leite, M. F. GPR91: expanding the frontiers of Krebs cycle intermediates. *Cell Commun. Signal.* **14**, 3 (2016).
- Sapieha, P. et al. The succinate receptor GPR91 in neurons has a major role in retinal angiogenesis. *Nat. Med.* **14**, 1067–1076 (2008).
- Vargas, S. L., Toma, I., Kang, J. J., Meer, E. J. & Peti-Peterdi, J. Activation of the succinate receptor GPR91 in macula densa cells causes renin release. *J. Am. Soc. Nephrol.* **20**, 1002–1011 (2009).
- Li, Y. H., Woo, S. H., Choi, D. H. & Cho, E. H. Succinate causes alpha-SMA production through GPR91 activation in hepatic stellate cells. *Biochem. Biophys. Res. Commun.* **463**, 853–858 (2015).
- McCreath, K. J. et al. Targeted disruption of the SUCNR1 metabolic receptor leads to dichotomous effects on obesity. *Diabetes* **64**, 1154–1167 (2015).
- Hakak, Y. et al. The role of the GPR91 ligand succinate in hematopoiesis. *J. Leukoc. Biol.* **85**, 837–843 (2009).
- Ryan, D. G. & O'Neill, L. A. J. Krebs cycle rewired for macrophage and dendritic cell effector functions. *FEBS Lett.* **591**, 2992–3006 (2017).
- Saraiva, A. L. et al. Succinate receptor deficiency attenuates arthritis by reducing dendritic cell traffic and expansion of Th17 cells in the lymph nodes. *FASEB J.* **12**, f201800285 (2018).
- Rubic-Schneider, T. et al. GPR91 deficiency exacerbates allergic contact dermatitis while reducing arthritic disease in mice. *Allergy* **72**, 444–452 (2017).
- Littlewood-Evans, A. et al. GPR91 senses extracellular succinate released from inflammatory macrophages and exacerbates rheumatoid arthritis. *J. Exp. Med.* **213**, 1655–1662 (2016).
- Peruzzotti-Jametti, L. et al. Macrophage-derived extracellular succinate licenses neural stem cells to suppress chronic neuroinflammation. *Cell Stem Cell* **22**, 355–368.e13 (2018).
- Lei, W. et al. Activation of intestinal tuft cell-expressed *Sucnr1* triggers type 2 immunity in the mouse small intestine. *Proc. Natl Acad. Sci. USA* **115**, 5552–5557 (2018).
- Shan, B. et al. The metabolic ER stress sensor IRE1 α suppresses alternative activation of macrophages and impairs energy expenditure in obesity. *Nat. Immunol.* **18**, 519–529 (2017).
- Manieri, E. & Sabio, G. Stress kinases in the modulation of metabolism and energy balance. *J. Mol. Endocrinol.* **55**, R11–R22 (2015).
- Arch, J. R., Hislop, D., Wang, S. J. & Speakman, J. R. Some mathematical and technical issues in the measurement and interpretation of open-circuit indirect calorimetry in small animals. *Int. J. Obes.* **30**, 1322–1331 (2006).
- Virtue, S. & Vidal-Puig, A. Assessment of brown adipose tissue function. *Front. Physiol.* **4**, 128 (2013).
- Mills, E. L. et al. Succinate dehydrogenase supports metabolic repurposing of mitochondria to drive inflammatory macrophages. *Cell* **167**, 457–470.e413 (2016).
- Hamilton, T. A., Zhao, C., Pavicic, P. G. Jr. & Datta, S. Myeloid colony-stimulating factors as regulators of macrophage polarization. *Front. Immunol.* **5**, 554 (2014).
- Jaguin, M., Houlbert, N., Fardel, O. & Lecureur, V. Polarization profiles of human M-CSF-generated macrophages and comparison of M1-markers in classically activated macrophages from GM-CSF and M-CSF origin. *Cell Immunol.* **281**, 51–61 (2013).
- Liao, X. et al. Kruppel-like factor 4 regulates macrophage polarization. *J. Clin. Invest.* **121**, 2736–2749 (2011).
- Luan, B. et al. CREB pathway links PGE2 signaling with macrophage polarization. *Proc. Natl Acad. Sci. USA* **112**, 15642–15647 (2015).

35. Avni, D., Ernst, O., Philosoph, A. & Zor, T. Role of CREB in modulation of TNF α and IL-10 expression in LPS-stimulated RAW264.7 macrophages. *Mol. Immunol.* **47**, 1396–1403 (2010).
36. Boutens, L. & Stienstra, R. Adipose tissue macrophages: going off track during obesity. *Diabetologia* **59**, 879–894 (2016).
37. Kwok, K. H., Lam, K. S. & Xu, A. Heterogeneity of white adipose tissue: molecular basis and clinical implications. *Exp. Mol. Med.* **48**, e215 (2016).
38. Qiu, Y. et al. Eosinophils and type 2 cytokine signaling in macrophages orchestrate development of functional beige fat. *Cell* **157**, 1292–1308 (2014).
39. Fabbiano, S. et al. Caloric restriction leads to browning of white adipose tissue through Type 2 immune signaling. *Cell Metab.* **24**, 434–446 (2016).
40. Hui, X. et al. Adiponectin enhances cold-induced browning of subcutaneous adipose tissue via promoting M2 macrophage proliferation. *Cell Metab.* **22**, 279–290 (2015).
41. Fujisaka, S. et al. Regulatory mechanisms for adipose tissue M1 and M2 macrophages in diet-induced obese mice. *Diabetes* **58**, 2574–2582 (2009).
42. Odegaard, J. I. et al. Alternative M2 activation of Kupffer cells by PPAR δ ameliorates obesity-induced insulin resistance. *Cell Metab.* **7**, 496–507 (2008).
43. Mills, E. L., Kelly, B. & O'Neill, L. A. J. Mitochondria are the powerhouses of immunity. *Nat. Immunol.* **18**, 488–498 (2017).
44. Trauelsen, M. et al. Receptor structure-based discovery of non-metabolite agonists for the succinate receptor GPR91. *Mol. Metab.* **6**, 1585–1596 (2017).
45. Mauer, J. et al. Signaling by IL-6 promotes alternative activation of macrophages to limit endotoxemia and obesity-associated resistance to insulin. *Nat. Immunol.* **15**, 423–430 (2014).
46. Reilly, S. M. & Saltiel, A. R. Countering inflammatory signals in obesity. *Nat. Immunol.* **15**, 410–411 (2014).
47. Pellegrinelli, V., Carobbio, S. & Vidal-Puig, A. Adipose tissue plasticity: how fat depots respond differently to pathophysiological cues. *Diabetologia* **59**, 1075–1088 (2016).
48. Carobbio, S., Pellegrinelli, V. & Vidal-Puig, A. Adipose tissue function and expandability as determinants of lipotoxicity and the metabolic syndrome. *Adv. Exp. Med. Biol.* **960**, 161–196 (2017).
49. Lumeng, C. N., DelProposto, J. B., Westcott, D. J. & Saltiel, A. R. Phenotypic switching of adipose tissue macrophages with obesity is generated by spatio-temporal differences in macrophage subtypes. *Diabetes* **57**, 3239–3246 (2008).
50. Wellen, K. E. & Hotamisligil, G. S. Obesity-induced inflammatory changes in adipose tissue. *J. Clin. Invest.* **112**, 1785–1788 (2003).

Acknowledgements

This study was supported by grants from the Spanish Ministry of Science, Innovation and Universities (PI14/00228 and PI17/01503 to J.V., SAF2015-65019-R to S.F.-V.,

SAF2014-56819-R and SAF2015-71878-REDT to A.C., BFU2016-78951-R to G.M.-M., PI15/00143 to C.S. and PI15/01562 to A.M., BFU2015-70454-REDT and BFU2017-90578-REDT to S.F.-V. and G.M.-M.) co-financed by the European Regional Development Fund (ERDF). The Spanish Biomedical Research Center in Diabetes and Associated Metabolic Disorders (CIBERDEM) (CB07708/0012) is an initiative of the Instituto de Salud Carlos III. N.K. is recipient of a predoctoral fellowship from MINECO, Spain (FPI, BES-2016-077745). C.S. acknowledges support from the 'Ramón y Cajal' program from MINECO (RYC2013-13186) and S.F.-V. the Miguel Servet tenure-track program (CP10/00438 and CPII16/00008) from the Fondo de Investigación Sanitaria, co-financed by the ERDF. We want to particularly acknowledge the patients and the BioBank IISPV (PT17/0015/0029) integrated in the Spanish National Biobanks Network for its collaboration. We also thank K. McCreath and A. Cervera for kindly providing the C57BL/6 *Sucnr1^{fl/fl}* mice and for their helpful comments on the manuscript. Finally, we thank IRB Barcelona Functional Genomics Core Facility for Microarray processing and IRB Barcelona Biostatistics and Bioinformatics facility.

Author contributions

J.V. and S.F.-V. conceived, designed and supervised the research project. N.K., V.C.-M. and E.C. participated in the conception and design of the study, sample collection, experiment planning and conduction. C.S. analyzed human metabolic data. M.E. performed flow cytometry data acquisition and analysis of data. M.I.H.-A. carried out transcriptome analysis. J.V.d.l.R. analyzed ChIP-seq genomic data. R.F. and R.J. participated in the human sample recruitment. D.H. provided technical assistance and analysis of data of the metabolic phenotype study in mice. C.N.-R., E.M.-M. and M.M.R. performed cell culture and technical animal procedures assistance. A.Z., A.C., A.M., G.M.-G. and C.S. provided scientific discussion and revised the manuscript. S.F.-V. and J.V. are the guarantors of this work.

Competing interests

The authors declare no competing interests.

Additional information

Supplementary information is available for this paper at <https://doi.org/10.1038/s41590-019-0372-7>.

Reprints and permissions information is available at www.nature.com/reprints.

Correspondence and requests for materials should be addressed to J.V. or S.F.

Publisher's note: Springer Nature remains neutral with regard to jurisdictional claims in published maps and institutional affiliations.

© The Author(s), under exclusive licence to Springer Nature America, Inc. 2019

Methods

Human cohort. All participants gave their informed consent and the study was reviewed and approved by the Ethics and Research Committee of Institut d'Investigació Sanitària Pere Virgili (IISPV CElm, Tarragona, Spain), in accordance with Good Clinical Practice Guidelines approved by the Health Department of Generalitat de Catalunya, which met all requirements of the Declaration of Helsinki. Donors were classified as lean or obese based on BMI following World Health Organization criteria. Plasma, scWAT and vWAT were obtained from age- and gender-matched human donors undergoing non-acute surgical interventions, such as hernia or cholecystectomy, in a scheduled routine surgery: lean $n = 15$ (BMI 22.87 ± 1.51); obese $n = 36$ (BMI 31.44 ± 4.55). Anthropometric and biochemical variables from the cohort are represented in Supplementary Table 3.

Mice. Myeloid cell-specific *Sucnr1* knockout mice (*LysM-Cre Sucnr1^{fl/fl}*) were generated by breeding *LysM-Cre* mice (kindly provided by G. Sabio, CNIC, Spain) with *Sucnr1^{fl/fl}* mice. *Cre*-negative *Sucnr1^{fl/fl}* littermates were used as controls. Mice were genotyped by PCR; genotyping of *Sucnr1^{fl/fl}* mice resulted in a 450-bp product for the *loxP*-targeted allele and a 300-bp product for the wild-type allele. All genotypes were generated on a pure C57BL/6 background. Total *Stat6^{-/-}* mice in a C57BL/6 background were purchased from The Jackson Laboratory. Mice were housed at the Faculty of Medicine and Health Science animal facility, Rovira i Virgili University (URV). Male mice were grouped (five per cage) under controlled conditions of 12 h light/dark cycle at 22 °C and ad libitum access to NCD (3.1% fat; SAFE diets, A04) or HFD (45% fat; Research diets, D12451), beginning at 7 weeks of age. All animal studies were supervised and approved by the Universitat Rovira i Virgili Animal Welfare and Ethics Committee. All animal procedures conformed to European Union Directive 86/609/EEC and recommendation 2007/526/EC regarding the protection of animals used for experimental and other scientific purposes, enacted under Spanish law 1201/2005.

Indirect calorimetry and activity measurements. Animals were placed in a comprehensive laboratory animal monitoring system (PhenoMaster, TSE Systems) for analysis of metabolic phenotypes of male *Sucnr1^{fl/fl}* and *LysM-Sucnr1^{fl/fl}* mice (at 22 °C), and at 22 °C, 30 °C and 8 °C for the cold-exposure study. Airflow rate was 380 ml min⁻¹; O₂ and CO₂ concentrations in room air and air leaving each cage were measured every 15 min. Energy expenditure (kcal h⁻¹ per mouse or kcal h⁻¹ kg⁻¹) was calculated from the amount of O₂ consumed (VO₂, ml h⁻¹ per mouse or ml h⁻¹ kg⁻¹, respectively) and the amount of CO₂ produced (VCO₂) using the equation energy expenditure (J) = 15.818VO₂ + 5.176VCO₂. The respiratory exchange ratio (RER) was calculated from the ratio VCO₂/VO₂. Activity, food and drink intake of each animal was calculated as described³¹. Data for energy expenditure were analyzed using analysis of covariance with body weight as a covariate.

Glucose and insulin tolerance test. After 16 h of fasting, mice were subjected to a glucose-tolerance test (GTT), receiving an intraperitoneal injection of glucose solution (1.5 g glucose per kg body weight). Blood was collected from the tail and glucose was measured using a handheld glucometer (Accu-Chek glucose reader; Roche). To measure insulin levels in response to glucose, blood was collected from tail punctures at 0, 15 and 30 min after injection and insulin was measured using a commercial Mouse Insulin Ultra-Sensitive ELISA (BioVendor). For the intraperitoneal insulin-tolerance test (ITT), mice were fasted for 3 h and injected with insulin (0.75 U kg⁻¹).

Isolation of mature adipocytes, SVF and ATMs. ATMs were isolated from the SVF of human adipose tissue biopsies as described^{52,53}. In brief, scWAT and vWAT was washed extensively with PBS to remove debris and treated with 0.1% collagenase in PBS and 1% BSA for 1 h at 37 °C with gentle agitation. Digested samples were centrifuged at 300g at 4 °C for 5 min to separate adipocytes from the SVF. Adipocytes were directly used for RNA isolation and the cell pellet containing the SVF was resuspended in red-blood-cell lysis buffer (10 mM KHCO₃, 150 mM NH₄Cl, 0.1 mM EDTA) for 2 min, then washed with PBS and passed through a 40 μm filter (Fisher Scientific). To isolate ultrapure ATMs, the SVF was incubated with F4/80 MicroBeads (130-110-443, MiltenyiBiotec) for 30 min and positive selection was performed with an autoMACS separator (MiltenyiBiotec). Each biologically independent sample was obtained from a pool of six to seven mice (*Sucnr1^{fl/fl}* or *LysM-Cre Sucnr1^{fl/fl}*), or two to three human individuals samples (lean or obese).

Isolation and culture of adipose tissue explants. Human adipose tissue samples were obtained as described above. Mouse scWAT and vWAT was freshly isolated and 0.2 g of tissue was placed in 1 ml DMEM/F12 and 10% fetal bovine serum (FBS). Samples were incubated for 24 h at 37 °C and 5% CO₂ without or with succinate at 200 μM. Each biologically independent sample was obtained from a pool of two to three mice (*Sucnr1^{fl/fl}* or *LysM-Cre Sucnr1^{fl/fl}*), or human individuals samples (lean or obese).

Flow cytometry. The SVF from scWAT and vWAT was isolated as described above. To isolate myeloid lineage cells, SVF was incubated with CD11b MicroBeads (130-049-601, MiltenyiBiotec) for 30 min, and positive selection was performed with an autoMACS separator. Magnetically isolated CD11b⁺ cells were washed and

incubated with the desired combination of fluorochrome-conjugated monoclonal antibodies, including FITC-anti-F4/80 (clone BM8), APC-anti-CD11c (clone N418), PE-anti-CD206 (clone MR6F3) and PE-Cy7-anti-Ly-6G (clone RB6-8C5) (all from eBiosciences) for 20 min. Data were acquired on a FACS Aria III (BD Biosciences) and analysis was performed using FACSDivaTM software (BD Biosciences).

Isolation and culture of human monocytes. Human PBMCs were isolated using Ficoll-Hypaque gradients (Amersham Bioscience). Monocytes were purified from PBMCs by magnetic cell sorting using CD14-microbeads (MiltenyiBiotec) as described⁵⁴. Human PBMC-derived Mφ were obtained by culturing CD14⁺ cells in RPMI medium supplemented with human recombinant M-CSF or GM-CSF (30 ng ml⁻¹; PeproTech) for 7 d at 37 °C, refreshed every 2 d. Each biologically independent sample was obtained from a pool of two to three human individuals samples.

Isolation of peritoneal macrophages. Mice were killed by CO₂ inhalation. Resident peritoneal cells were harvested by lavage with 5 ml ice-cold PBS as described⁵⁵. At 72 h, cells mainly comprised peritoneal macrophages⁵⁶. Macrophages were purified by adherence to tissue culture plates using an established procedure that gives >90% purity⁵⁶. Non-adherent cells were removed by washing twice with PBS. Each biologically independent sample was obtained from a pool of six to seven mice (*Sucnr1^{fl/fl}* or *LysM-Cre Sucnr1^{fl/fl}*).

Isolation of BMDMs. BMDMs from 8- to 11-week-old mice were obtained as described⁵⁷. In brief, mice were killed by CO₂ and the femurs and tibiae were collected and ground gently with a sterile mortar in 5 ml ice-cold PBS. Supernatants were collected in ice-cold PBS and filtered through a 70 μm nylon cell strainer to remove solid fragments. The filtrate was centrifuged at 450g for 10 min at 4 °C, and pellets were dissociated in 10 ml red-blood-cell lysis buffer for 30 sec. After centrifugation, the pellet was dissociated in 20 ml of RPMI, 10% FBS and 1% antibiotic/antimycotic solution at 37 °C, and cultured in 100 mm Petri-dishes for 4 h at 37 °C to remove resident bone marrow macrophages by adhesion. Collected supernatants were filtered and centrifuged as described above. Pellets were dissociated in RPMI supplemented with murine recombinant M-CSF or GM-CSF (30 ng ml⁻¹) and harvested after 7 d at 37 °C with 5% CO₂. Media and stimuli were refreshed every 2 d. Cells were placed in RPMI medium without stimulus for 24 h before treatments. Differentiation was confirmed by F4/80 expression using flow cytometry (data not shown). Each biologically independent sample was obtained from a pool of six to seven mice (*Sucnr1^{fl/fl}* or *LysM-Cre Sucnr1^{fl/fl}*).

THP1 cell culture. The human monocyte THP1 cell line was obtained from the ATCC. Cells were cultured as described⁵³. In brief, cells were cultured in RPMI-1640 medium supplemented with 10% FBS and 1% antibiotic/antimycotic solution in a humidified cell culture incubator at 37 °C with 5% CO₂.

Macrophage differentiation and stimulation. To assess gene expression of pro- and anti-inflammatory markers, human PBMCs and murine BMDMs treated with M-CSF were stimulated with *Escherichia coli*-derived lipopolysaccharide (serotype 0111:B4, number L4391, Sigma-Aldrich) (250 ng ml⁻¹) or human or murine recombinant IL-4 (PeproTech) (30 ng ml⁻¹), respectively, for 24 h. For succinate (200 μM), lipopolysaccharide (250 ng ml⁻¹) or IL-4 (30 ng ml⁻¹) treatment of ATMs, peritoneal macrophages and THP1, cells were stimulated for 6 h. For cell-signaling studies, BMDMs^{M-CSF} were untreated or pre-incubated with a PKA inhibitor (H-89; number 037M4702V, Sigma-Aldrich) (50 μM) for 30 min and/or succinate (200 μM) for 2 h and subsequently exposed to IL-4 for the indicated time points. For succinate signaling, cells were untreated or pretreated with H-89 and then stimulated with succinate for the indicated time points.

STAT6 and KLF4 silencing. THP1 cells were transfected with human STAT6 siRNA (number 6778), KLF4 siRNA (number 9314) or a control (non-targeting pool, number 16600) using Dharmafect transfection reagent diluted in Opti-MEM I reduced serum medium (Invitrogen), added to the cultured cells for 48–72 h. BMDMs and ATMs were transfected with mouse STAT6 siRNA (number 20852), KLF4 siRNA (number 16600) or a control (Accell non-targeting pool, number D-001910-1050) using Accell siRNA delivery media (number B-005000-100), added to the cultured cells for 48–72 h. siRNAs were purchased from Dharmacon.

Succinate determination. Succinate levels were measured in plasma from humans and mice and also from conditioned medium from human PBMCs and murine BMDMs after 24 h culture without stimuli with the EnzyChrom™ Succinate Assay Kit (BioAssay Systems), as described¹¹. The assay sensitivity was 12 μM and the intra- and interassay co-efficient of variances were less than 3.5 and 6.95%, respectively. Succinate intracellular levels were measured with the Succinate Colorimetric Assay kit (Sigma-Aldrich).

Gene-expression analysis. Total RNA was extracted from tissues/cells using the RNeasy Lipid Tissue Mini Kit (Qiagen Science). Total RNA quantity was measured at 260 nm and purity was assessed by the optical density 260 nm/optical

density 280 nm ratio. One microgram of RNA was transcribed to complementary DNA with random primers using the Reverse Transcription System (Applied Biosystems). Quantitative gene expression was evaluated by qPCR on a 7900HT Fast Real-Time PCR System using the TaqMan Gene Expression Assay (Applied Biosystems) (Supplementary Table 4). Results were calculated using the comparative C_T method ($2^{-\Delta\Delta C_T}$), and expressed relative to the expression of the housekeeping gene 18S for human samples, and beta-2-microglobulin for murine samples.

Microarray analyses. RNA isolation, library preparation and amplification from *Sucnr1*^{fl/fl} and *LysM-Sucnr1*^{fl/fl} ATMs from scWAT and vWAT were performed as described⁵⁸. 8 μ g of cDNA was subsequently fragmented, labeled and hybridized to MG-430 PM array strip (Thermo Fisher Scientific, Affymetrix, reference 901570). Processing of microarray samples was carried out using packages *affy*⁵⁹ and *affyplm*⁶⁰ from Bioconductor. Raw cell files were normalized using robust multi-array average (RMA) background correction and summarization⁶¹. Technical metrics PM median, PM interquartile range (IQR), RMA IQR and RNA degradation described in ref.⁶² were computed and recorded as additional features for each sample. Differential expression between conditions was calculated using the moderated *t*-statistic by empirical Bayes shrinkage⁶³. Experiment pool and Eklund metric RMA IQR were included as adjusting variables in the model to correct for technical variability. The normalized expression matrix was adjusted by the effect of the experiment pool and RMA IQR variables. This matrix was scaled and used afterwards to generate individual gene heat maps. The \log_2 fold-change information (positive change when *LysM* was higher than flox/flox and negative change when *LysM* was lower than flox/flox) was considered to rank all genes in the genome, and GSEA was performed using the Broad Institute's implementation⁶⁴ on MSigDB Hallmark collections. Hallmark gene sets were translated to mouse homologs using Biomart⁶⁵. Statistically enriched Hallmark gene sets were also identified using the standard hypergeometric test. Significance was defined at levels of adjusted *P* value smaller than four thresholds, that is, 0.25, 0.10, 0.05 and 0.01, using the Benjamini–Hochberg multiple testing correction. Pools of four animals from each genotype (*Sucnr1*^{fl/fl} or *LysM-Cre Sucnr1*^{fl/fl}) were employed to obtain each experiment.

Immunoblot analysis. Cells were lysed and homogenized in M-PER buffer containing Protease Inhibitor Cocktail, and protein concentration was determined with the BCA Protein Assay Kit (both from Pierce Biotechnology). Equal amounts of total protein were separated using SDS-polyacrylamide gel electrophoresis, transferred to Immobilon membranes and blocked. Immunoblot analysis was performed through the use of polyclonal antibodies against phospho-SAPK/JNK, phospho-CREB, phospho-STAT6, phospho-PKA, STAT6 and KLF4, from Cell Signaling Technology; polyclonal antibodies against IL-10 and a monoclonal antibody for UCP1, from Abcam; polyclonal antibodies against SUCNR1 and GAPDH from Sigma-Aldrich and FAA from Santa Cruz Biotechnology. FAA and GAPDH were used as loading controls. Immunoreactive bands were visualized with SuperSignal West Femto chemiluminescent substrate (Pierce) and images were captured using the VersaDoc imaging system and Quantity One software (BioRad).

Histology. Sections of 5 μ m thickness were paraffin-embedded and prepared for hematoxylin and eosin staining or for UCP1 or F4/80 immunohistochemistry. In brief, paraffin sections were de-paraffinized and rehydrated. For UCP1 detection, heat-induced antigen retrieval of sections was carried out using Tris-buffer solution (pH 9) or citrate (pH 6) for F4/80. Slides were blocked 1 h in blocking buffer, incubated at 4 °C overnight with the primary rabbit anti-mouse UCP1 (Abcam) or rat anti-mouse F4/80 (BioRad) antibody, followed by incubation with a donkey anti-rabbit IgG against UCP1 (GE Healthcare) or a goat anti-rat against F4/80 (Vector Laboratories) horseradish peroxidase-conjugated antibody for 90 min at room temperature. Slides were washed thoroughly and coverslips were mounted with DPX mounting medium (Sigma-Aldrich). Sections were observed by microscopy on a Leica DM1000 microscope and image acquisition was performed using Leica microsystems imaging software.

***Sucnr1* promoter study through bioinformatic analysis.** Chromatin immunoprecipitation with sequencing (ChIP-seq) sequencing data from BMDMs, published by Ostuni et al.⁶⁶, were aligned to the University of California Santa Cruz mm9 murine genome using bowtie2 aligner software (v.2.2.9)⁶⁷. Data analysis was performed using HOMER software suite (v.4.9) (<http://homer.ucsd.edu/homer/>) described in Heinz et al.⁶⁸ Each ChIP-seq experiment was normalized to a total number of 10⁷ uniquely mapped tags. Aligned read files were visualized by obtaining snapshot tracks from UCSC Genome browser. To identify STAT6 DNA-binding motifs, we obtained four sequences found in STAT6 binding sites (1,000 bp surrounding STAT6 peaks) from *Sucnr1* (one sequence) and known classic STAT6 targets arginase-1 (two sequences) and chitinase-like protein 3 (one sequence). Sequence motif obtained with MEME-ChIP v.4.12.0 software suite⁶⁹ was interrogated to TOMTOM tool to evaluate similarities to known transcription factor binding motifs. MEME-ChIP *P* value indicates the probability that an equal or better site would be found in a random sequence of the same length conforming to the background letter frequencies; TOMTOM *P* value indicates the probability

that a random motif of the same width as the target would have an optimal alignment with a match score as good or better than the target's. Tomtom estimates the *P* value using a null model consisting of sampling motif columns from all the columns in the set of target motifs.

Statistical analysis. Each experiment was performed two, three or four times and pooled to carry out statistical analysis. For in vitro data, values are reported as mean \pm s.e.m. Differences between groups were determined using unpaired *t*-test (two-tailed, 95% confidence interval), and statistical significance in body weight, GTT and ITT curves were tested by two-way analysis of variance, using GraphPad Prism 5 software. *P* < 0.05 was considered significant. For clinical and anthropometrical variables the Kolmogorov–Smirnov test and Shapiro–Wilk test were used to test normality of variables. Normally distributed data were expressed as mean \pm s.d., and for variables with no Gaussian distribution values were expressed as median (25th–75th quartiles). Statistical significance was tested by unpaired *t*-test (two-tailed, 95% confidence interval) or Mann–Whitney *U* test. To analyze the differences in nominal variables between groups, we used the χ^2 test. Pearson's and Spearman's correlation coefficients (two-tailed, 95% confidence interval) with Bonferroni adjustment were used to analyze the relationship between parameters. All clinical data were analyzed using Statistical Package for the Social Sciences software, v.15 (SPSS).

Reporting Summary. Further information on research design is available in the Nature Research Reporting Summary linked to this article.

Data availability

Full scans for all immunoblots and source data for Figs. 1–8 are provided in the Supplementary Information. All other data are available from the corresponding authors upon request. All microarray data are in the GEO database with accession code GSE120121.

References

- Medina-Gomez, G. et al. PPAR gamma 2 prevents lipotoxicity by controlling adipose tissue expandability and peripheral lipid metabolism. *PLoS Genet.* **3**, e64 (2007).
- Ceperuelo-Mallafre, V. et al. Adipose tissue glycogen accumulation is associated with obesity-linked inflammation in humans. *Mol. Metab.* **5**, 5–18 (2016).
- Serena, C. et al. Obesity and Type 2 diabetes alters the immune properties of human adipose derived stem cells. *Stem Cells* **34**, 2559–2573 (2016).
- Maymo-Masip, E. et al. The rise of soluble TWEAK levels in severely obese subjects after bariatric surgery may affect adipocyte-cytokine production induced by TNF α . *J. Clin. Endocrinol. Metab.* **98**, E1323–E1333 (2013).
- Gilmour, J. S. et al. Local amplification of glucocorticoids by 11 beta-hydroxysteroid dehydrogenase type 1 promotes macrophage phagocytosis of apoptotic leukocytes. *J. Immunol.* **176**, 7605–7611 (2006).
- Zhang, X., Goncalves, R. & Mosser, D. M. The isolation and characterization of murine macrophages. *Curr. Protoc. Immunol.* Ch. 14, Unit 11 (2008).
- Trouplin, V. et al. Bone marrow-derived macrophage production. *J. Vis. Exp.* **81**, e50966 (2013).
- Gonzalez-Roca, E. et al. Accurate expression profiling of very small cell populations. *PLoS ONE* **5**, e14418 (2010).
- Gautier, L., Cope, L., Bolstad, B. M. & Irizarry, R. A. *affy*—analysis of Affymetrix GeneChip data at the probe level. *Bioinformatics* **20**, 307–315 (2004).
- Heber, S. & Sick, B. Quality assessment of affymetrix genechip data. *OMICS* **10**, 358–368 (2006).
- Irizarry, R. A. et al. Exploration, normalization, and summaries of high density oligonucleotide array probe level data. *Biostatistics* **4**, 249–264 (2003).
- Eklund, A. C. & Szallasi, Z. Correction of technical bias in clinical microarray data improves concordance with known biological information. *Genome Biol.* **9**, R26 (2008).
- Ritchie, M. E. et al. limma powers differential expression analyses for RNA-sequencing and microarray studies. *Nucleic Acids Res.* **43**, e47 (2015).
- Subramanian, A. et al. Gene set enrichment analysis: a knowledge-based approach for interpreting genome-wide expression profiles. *Proc. Natl Acad. Sci. USA* **102**, 15545–15550 (2005).
- Durinck, S., Spellman, P. T., Birney, E. & Huber, W. Mapping identifiers for the integration of genomic datasets with the R/Bioconductor package biomaRt. *Nat. Protoc.* **4**, 1184–1191 (2009).
- Ostuni, R. et al. Latent enhancers activated by stimulation in differentiated cells. *Cell* **152**, 157–171 (2013).
- Langmead, B. & Salzberg, S. L. Fast gapped-read alignment with Bowtie 2. *Nat. Methods* **9**, 357–359 (2012).
- Heinz, S. et al. Simple combinations of lineage-determining transcription factors prime cis-regulatory elements required for macrophage and B cell identities. *Mol. Cell* **38**, 576–589 (2010).
- Bailey, T. L. et al. MEME SUITE: tools for motif discovery and searching. *Nucleic Acids Res.* **37**, W202–W208 (2009).

Reporting Summary

Nature Research wishes to improve the reproducibility of the work that we publish. This form provides structure for consistency and transparency in reporting. For further information on Nature Research policies, see [Authors & Referees](#) and the [Editorial Policy Checklist](#).

Statistics

For all statistical analyses, confirm that the following items are present in the figure legend, table legend, main text, or Methods section.

- | | |
|-----|-----------|
| n/a | Confirmed |
|-----|-----------|
- The exact sample size (n) for each experimental group/condition, given as a discrete number and unit of measurement
 - A statement on whether measurements were taken from distinct samples or whether the same sample was measured repeatedly
 - The statistical test(s) used AND whether they are one- or two-sided
Only common tests should be described solely by name; describe more complex techniques in the Methods section.
 - A description of all covariates tested
 - A description of any assumptions or corrections, such as tests of normality and adjustment for multiple comparisons
 - A full description of the statistical parameters including central tendency (e.g. means) or other basic estimates (e.g. regression coefficient) AND variation (e.g. standard deviation) or associated estimates of uncertainty (e.g. confidence intervals)
 - For null hypothesis testing, the test statistic (e.g. F , t , r) with confidence intervals, effect sizes, degrees of freedom and P value noted
Give P values as exact values whenever suitable.
 - For Bayesian analysis, information on the choice of priors and Markov chain Monte Carlo settings
 - For hierarchical and complex designs, identification of the appropriate level for tests and full reporting of outcomes
 - Estimates of effect sizes (e.g. Cohen's d , Pearson's r), indicating how they were calculated

Our web collection on [statistics for biologists](#) contains articles on many of the points above.

Software and code

Policy information about [availability of computer code](#)

Data collection

Indirect calorimetry and activity measurements: PhenoMaster, TSE Systems, Germany
 Flow cytometry: FACS Aria III (BD Biosciences)
 Gene expression analysis: 7900HT Fast Real-Time PCR System using the TaqMan® Gene Expression Assay (Applied Biosystems) Software: RQ Manager 1.2. Ink
 Microarray analysis: IMG-430 PM array strip (Thermo Fisher Scientific, Affymetrix, Ref; 901570)
 Image collection software: Quantity One 4.6.6 (Basic), Leica microsystems imaging (O2614F869 Leica Hardware Configurator 17.10.7879.3-2017.2.0) LASV4.13

Data analysis

FACSDivaTM software (6.1.3; BD Biosciences) for flow cytometry studies
 GraphPad Prism 6 software and Statistical Package for the Social Sciences software, version 15 (SPSS, Chicago, IL) for statistical analysis Packages.
 Affy (1.59.1), affyplm (1.57.0) and Biomart (2.37.5) from Bioconductor, GSEA tool - gsea2 (2.0.12), pre ranked version, from Broad Institute for microarray analysis.
 Bowtie2 aligner software (v2.2.9); HOMER software suite (v4.9) (<http://biowhat.ucsd.edu/homer/>) and MEME-ChIP v. 4.12.0 software suite for bioinformatic analysis of Sucnr1 promoter

For manuscripts utilizing custom algorithms or software that are central to the research but not yet described in published literature, software must be made available to editors/reviewers. We strongly encourage code deposition in a community repository (e.g. GitHub). See the Nature Research [guidelines for submitting code & software](#) for further information.

Data

Policy information about [availability of data](#)

All manuscripts must include a [data availability statement](#). This statement should provide the following information, where applicable:

- Accession codes, unique identifiers, or web links for publicly available datasets
- A list of figures that have associated raw data
- A description of any restrictions on data availability

Full scans for all western blots and source data of figures 1-8 are provided in supplementary information. All other data that support the findings of this study are available from the corresponding authors upon request. All microarray data are in the GEO database with accession code GSE120121 (submitted to GEO repository).

Field-specific reporting

Please select the one below that is the best fit for your research. If you are not sure, read the appropriate sections before making your selection.

- Life sciences Behavioural & social sciences Ecological, evolutionary & environmental sciences

For a reference copy of the document with all sections, see [nature.com/documents/nr-reporting-summary-flat.pdf](https://www.nature.com/documents/nr-reporting-summary-flat.pdf)

Life sciences study design

All studies must disclose on these points even when the disclosure is negative.

Sample size	Pilot studies were used for estimation of the sample size. In most of the in vivo experiments, 6 to 10 mice was sufficient to identify differences between groups with at least 95% power and a 5% significance level.
Data exclusions	No exclusion criteria were pre-established. For in vivo experiments and clinical analysis outliers were excluded. The criteria used to identify outliers was any data point more than 1.5 interquartile ranges (IQRs) below the first quartile or above the third quartile. For in vitro studies: In figure 3a-c one biological replicate was excluded for not achieving a suitable polarization according to typical pro-inflammatory and anti-inflammatory macrophage markers. Outliers were excluded in figures:1g, 1h, 2h, 2i, 3g, 5d, 5e, 7a and supplementary 2e
Replication	For in vitro data each experiment was repeated at least 3 times as indicated in each figure. For ex vivo studies with human explants data from two independent experiments (derived from pool of 4 lean and 4 obese subjects). All attempt to replicate the reported experiment were successful.
Randomization	Mice were organized as control or KO group based on genotyping. Nonetheless, during housing littermate animals of the same sex (irrespective of whether they are control or ko) were in the same cage to avoid any bias due to location. In the in vitro and in vivo experiments samples were allocated randomly. To control for covariates between cell preparations (e.g. BMDMs and ATMs) we have pooled the generated cells from different mice together.
Blinding	For in vivo experiments the researcher doing the experiment was blinded about genotype. At the end of the experiments a second investigator identified the genotypes and performed data analysis. In the qPCR and flow cytometry experiments investigators responsible for data collection had no knowledge of sample information. Data analysis was performed by a second investigator blind for samples allocations.

Reporting for specific materials, systems and methods

We require information from authors about some types of materials, experimental systems and methods used in many studies. Here, indicate whether each material, system or method listed is relevant to your study. If you are not sure if a list item applies to your research, read the appropriate section before selecting a response.

Materials & experimental systems

n/a	Involved in the study
<input type="checkbox"/>	<input checked="" type="checkbox"/> Antibodies
<input type="checkbox"/>	<input checked="" type="checkbox"/> Eukaryotic cell lines
<input checked="" type="checkbox"/>	<input type="checkbox"/> Palaeontology
<input type="checkbox"/>	<input checked="" type="checkbox"/> Animals and other organisms
<input type="checkbox"/>	<input checked="" type="checkbox"/> Human research participants
<input checked="" type="checkbox"/>	<input type="checkbox"/> Clinical data

Methods

n/a	Involved in the study
<input checked="" type="checkbox"/>	<input type="checkbox"/> ChIP-seq
<input type="checkbox"/>	<input checked="" type="checkbox"/> Flow cytometry
<input checked="" type="checkbox"/>	<input type="checkbox"/> MRI-based neuroimaging

Antibodies

Antibodies used

phospho-SAPK/JNK (Cell Signaling, Cat #9251S, Lot# 26, 1:1000 dilution)
 phospho-CREB (Cell Signaling, Cat#9198S, Lot# 14 ,1:1000 dilution)
 phospho-STAT6 (Cell Signaling, Cat#56554S, Lot# 1, 1:1000 dilution)
 phospho-PKA –C (Cell Signaling, Cat#4781S, Lot#9, 1:1000 dilution)
 STAT-6 (Cell Signaling, Cat#9362S, Lot#5 , 1:1000 dilution)
 KLF4 (Cell Signaling, Cat#4038S, Lot# 3, 1:1000 dilution)
 Anti- IL10 (Clone JES 5-2A5, Abcam, Cat# ab33471, Lot# GR3190734-4, 1:500 dilution)
 UCP1 (Abcam, Cat# ab33471, Lot# GR249119-10, 1:1000 dilution)
 SUCNR1 (Sigma , Cat#SAB4502428, Lot# 61748 , 1:500 dilution)
 Anti-GAPDH (Sigma , Cat#GW22763-50ug, Lot# 118k1808V, 1:1000 dilution)
 Fumarylacetoacetase(C-20, Santa cruz, Cat#sc-66223, Lot # F1815, 1:1000 dilution)

Secondary

Anti-Rabbit IgG Horseradish Peroxidase-Linked (GE Healthcare, Cat#NA934, Lot#16897770, 1:2000 dilution)
 Goat Anti-Rat (abcam, Cat# ab205720, Lot# GR3233762-1, 1:2000 dilution)
 Goat IgG Horseradish Peroxidase-Conjugated(R&D Systems, Cat#HAF109, Lot#XGD1016011, 1:2000 dilution)
 Rabbitt Anti-Chicken IgY (abcam, Cat#ab6753, Lot#GR4712560, 1:2000 dilution)

Cytometry

FITC-anti-F4/80 (clone BM8, eBiosciences, Cat#11-4801-81, Lot#4318482, 0.5ug/test)
 APC-anti-CD11c (clone N418, eBiosciences, Cat# 17-0114-81, Lot#4307369, 0.25ug/test)
 PE-anti-CD206 (cloneMR6F3, eBiosciences, Cat# 12-2061-80, Lot#4336333, 0.125ug/test)
 PE-Cy7-anti-Ly-6G (clone RB6-8C5, eBiosciences, Cat# 25-5931-82, Lot#4331170, 0.125ug/test)

Validation

All antibodies used in western blot experiments have validation statement provided on the website of the manufacturer and are largely described in the literature.

For flow cytometry experiment all antibodies were validated using appropriate FMO/isotype controls. Compensation was performed in each batch of experiments with Anti-Rat and Anti-Hamster Ig κ /Negative Control Compensation Particles Set (BD™ CompBeads) . Cells were analyzed or sorted with a BD FACS Aria III with 70- μ m nozzle and running DiVa software (BD Bioscience) and analyzed with FlowJo software (version 10.5).

Eukaryotic cell lines

Policy information about [cell lines](#)

Cell line source(s)

The source of the human monocyte THP-1 cell line is American Type Culture Collection (ATCC).

Authentication

THP-1 cells is a well established cell line, no in house authentication has been done.

Mycoplasma contamination

THP-1 cell line were routinely tested for mycoplasma contamination (once every two months aprox). Only micoplasma-free cells were used for the experiments.

Commonly misidentified lines (See [ICLAC](#) register)

No misidentified cell lines have been used in this study

Animals and other organisms

Policy information about [studies involving animals](#); [ARRIVE guidelines](#) recommended for reporting animal research

Laboratory animals

Male and female Sucnr1fl/fl, LysM-Cre Sucnr1fl/fl or Stat6^{-/-} animals, 7-27 weeks old. All genotypes were generated on a pure C57BL/6 background. Mice were housed at the Faculty of Medicine and Health Science (FMCS) animal facility from Rovira i virgili University (URV). Male mice were grouped (5 per cage) under controlled conditions of 12 hr light/dark cycles at 22oC and ad libitum access to NCD (SAFE diets, A04) or a HFD (Research diets, D12451), beginning at 7 weeks of age. More details are reported in Methods.

Wild animals

No wild animals were used for this study

Field-collected samples

This study did not involve field-collected samples

Ethics oversight

All studies in mice were approved by the local ethics committee. All animal procedures conformed to EU Directive 86/609/EEC and recommendation 2007/526/EC regarding the protection of animals used for experimental and other scientific purposes, enacted under Spanish law 1201/2005.

Human research participants

Policy information about [studies involving human research participants](#)

Population characteristics	Anthropometric and biochemical variables from the subjects used in this study are specified in supplementary table 3. Donors were classified as lean or obese based on body mass index (BMI) following World Health Organization criteria. 29 females and 22 males, average age=54.
Recruitment	Donors were recruited in the Ambulatory Surgery Unit of University Hospital Joan XXIII. Plasma, scWAT and vWAT were obtained from age- and gender-matched human donors undergoing non-acute surgical interventions, such as hernia or cholecystectomy, in a scheduled routine surgery.
Ethics oversight	All participants gave their informed consent and the study was reviewed and approved by the Ethics and Research Committee of Institut d'Investigació Sanitària Pere Virgili (IISPV CEIm, Tarragona, Spain), in accordance with Good Clinical Practice Guidelines approved by the Health Department of Generalitat de Catalunya, which met all requirements of the Declaration of Helsinki.

Note that full information on the approval of the study protocol must also be provided in the manuscript.

Flow Cytometry

Plots

Confirm that:

- The axis labels state the marker and fluorochrome used (e.g. CD4-FITC).
- The axis scales are clearly visible. Include numbers along axes only for bottom left plot of group (a 'group' is an analysis of identical markers).
- All plots are contour plots with outliers or pseudocolor plots.
- A numerical value for number of cells or percentage (with statistics) is provided.

Methodology

Sample preparation	Adipose tissue from mice was dissected and digested with collagenase. Digested samples were centrifuged and the pellet contains our sample, the stroma-vascular fraction (SVF). SVF was resuspended in red-blood-cells lysis buffer and to isolate adipose tissue macrophages (ATMs,) SVF was incubated with CD11b MicroBeads (MiltenyiBiotec) for 30 min, and positive selection was performed by autoMACS separator. Magnetically isolated CD11b+ cells were washed and incubated with FITC-anti-F4/80 (clone BM8, eBiosciences), APC-anti-CD11c (clone N418, eBiosciences), PE-anti-CD206 (clone MR6F3, eBiosciences) and PE-Cy7-anti-Ly-6G (clone RB6-8C5, eBiosciences) for 20 min at room temperature, the preparation was washed and resuspended in 400 µl of PBS before analysis.
Instrument	FACS Aria III (BD Biosciences) serial number P28200182
Software	FACSDiva software (BD Biosciences)
Cell population abundance	Due to the mid-low abundance of ATMs in the SVF in normal conditions, we added a concentration step in the sample preparation by previous isolation of CD11b+ cells. This sample preparation allowed us to work with a higher abundance and trustworthiness.
Gating strategy	Each experiment has an extra compensatory step using compensation bead (BD CompBeads) to harmonize the antibodies used in the experiment. The gating strategy started with the typical FSC/SSC separation followed by SSC-H/SSC-W to obtain a population of single cells. Positive cells were defined in a dot-plot of FITC-F4/80 vs other fluorochromes such as PE-CD206, APC-CD11c or PE-Cy7-Ly6G by previously running a blank sample to set the auto-fluorescence of the cells.

- Tick this box to confirm that a figure exemplifying the gating strategy is provided in the Supplementary Information.